

POLITECNICO DI TORINO

Corso di Laurea in Ingegneria Biomedica

Tesi di Laurea Magistrale

Surface structuring of a titanium alloy for contact
with soft tissues



Relatrici:

Prof.ssa Silvia Spriano
Prof.ssa Sara Ferraris

Candidata:

Giulia Camera

Aprile 2018

Contents

Introduction.....	1
1. Soft tissue implant contact	2
1.1 Tooth anatomy [1].....	2
1.2 Fibroblasts.....	4
1.3 Dental implant.....	5
1.4 Implant success and durability.....	7
1.5 Peri-implant and periodontal soft tissue.....	9
1.6 Peri-implant mucositis and peri-implantitis.....	10
1.7 Oral cavity bacteria	12
1.8 Osseointegration.....	14
2. Titanium and Titanium alloys	16
2.1 Biomaterial.....	16
2.2 Titanium	18
2.3 Titanium alloy.....	20
2.4 Ti15Mo.....	23
2.5 Electron Beam Welding (EBW)	26
3. Surface micro/nano structuring.....	28
3.1 In vivo cell-matrix interaction.....	28
3.1.1 Extracellular matrix structure and function (ECM).....	28
3.1.2 Cell membrane structure and function	29
3.1.3 Cell-ECM adhesion.....	30
3.2 In vitro cell-matrix interaction	31
3.3 Effect of micro and nano topography on cells	31
3.4 Bacteria-matrix interaction	36
3.5 Optimal grooves for fibroblast.....	38
4. Materials and methods	40
4.1 Sample preparation	40
4.2 Electron beam (EBW).....	42
4.3 Cutting of samples	44
4.4 Dilatometry	45
4.5 Furnace.....	47
4.5 Metallography	48
4.6 Sample washing and sterilization.....	49
4.7 Cell and bacteria test.....	51
4.8 Characterisation methods.....	52
4.8.1 Scanning Electron Microscope (SEM)	52

4.8.2 Surface roughness	53
4.8.3 AFM	55
4.8.4 Contact angle.....	56
4.8.5 XRD [55].....	58
5. Results and discussion	61
5.1 SEM analysis after Electron Beam	61
5.2 SEM analysis after heat treatment	62
5.2.1 SEM images after dilatometry	62
5.2.2 SEM images after furnace.....	65
5.3 Etching	67
5.4 Surface roughness	69
5.5 AFM.....	72
5.6 Contact angle.....	Errore. Il segnalibro non è definito.
5.7 XRD	76
5.8 Cell and bacteria test	79
Conclusion and future works	82
Bibliography.....	84

Introduction

In order to guarantee the success of an implant, it is essential that it reaches primary and secondary stability and is therefore perfectly integrated in the host tissue without the presence of micromovements between implant and bone. For dental implants, however, soft tissue contact is still a problem. In this area, in fact, the adhesion and proliferation of bacteria can lead to the onset of infections such as peri-implant mucositis and peri-implantitis, which can lead to implant failure. It has been demonstrated by several authors that the superficial topography of an implant can promote cellular adhesion and inhibit bacterial adhesion, influencing primary and secondary stability and therefore determining the success of an implant.

In the field of implantology, titanium and its alloys are the most widely used materials due to their characteristics of low density, high strength, low modulus of elasticity, low thermal conductivity, low thermal expansion, excellent corrosion resistance, ease of processing and excellent biocompatibility.

In this thesis work, surface topography modifications were carried out on samples of a beta stabilizing alloy Ti15Mo in order to evaluate cellular and bacterial adhesion.

Molybdenum is a non-toxic and non-allergic element that makes it possible to obtain titanium alloys with low modulus of elasticity and high strength. Moreover, thanks to Mo concentrations greater than 10% it is possible to obtain a very fine and homogeneous microstructure, made up of small and equiaxial beta grains.

In this context, Electron beam welding (EBW) was used to make microgrooves of 10 and 30 μm by modifying the surface of the samples. Following EBW, some samples were subjected to thermal treatments that caused a change in the microstructure of the material: it was possible to observe the precipitation of the alpha phase.

Both types of samples (subject to heat and non-heat treatment) were then subjected to superficial characterization (SEM, LOM, Surface roughness, AFM, wettability, XRD) and cell and bacterial tests to estimate the efficiency of the changes made.

1. Soft tissue implant contact

1.1 Tooth anatomy [1]

The teeth are small chewing organs made up of four types of tissue: two superficial (i. e. enamel and cement) and two deep (i. e. dentin and pulp). The enamel covers the visible and protruding part of the gum of the tooth, i. e. the crown, while the cement covers the invisible and sharply shaped part, i. e. the root, contained in the dental alveoli (cavity of the maxillary bone); moreover, both are subtended by the dentin. The pulp is contained in a central cavity extending from crown to root and communicating with the periodontium (at root level) through an apical hole. The border between crown and root is the neck.

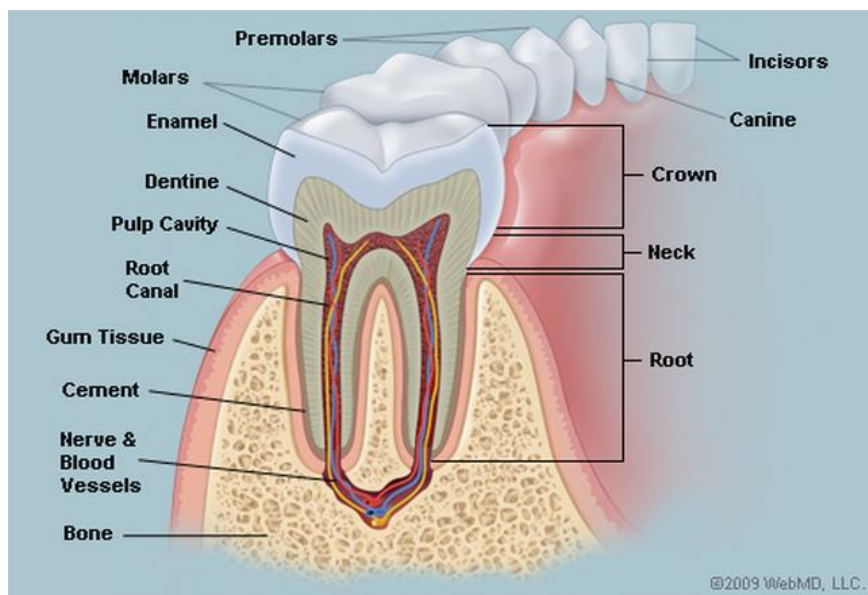


Figure 1.1: Tooth anatomy

From the functional and embryological point of view enamel, dentin and pulp are true tooth tissues. Instead, cement, periodontal ligament and gingiva constitute the periodontium.

Enamel is a tissue of epithelial origin without vessels and nerve endings. It is an acellular tissue that is consumed with age (the ameloblasts, once the enamel production is complete, are atrophic). Enamel is also very hard (it is the hardest in the human body) due to its high mineralisation; 96 % of the inorganic material consists of hydroxyapatite crystals organised into enamel prisms and 3-4 % of water.

Dentin, separated from the enamel by a wavy and irregular line (the enamel-dentin junction) is a mineralized avascular tissue (collagen fibres) that circumscribes the pulp cavity: it subtends the enamel at crown level and the cement at root level. It is a harder tissue than compact bone, with predominantly inorganic intercellular substance. The formation of dentin is preceded by the deposition and subsequent mineralization of predentine, a substance not calcified and perennially present in the tooth; in this way the production of dentin is always continuous.

Pulp is a highly vascularized and innervated connective tissue contained in the pulp cavity of the crown and root canal. It differs from other connective tissues due to the presence of odontoblast (the dentin cells used to produce the intercellular substance); it also contains the dental pulp, rich in collagen.

Cement and alveolar bone tissue (hard tissues), periodontal ligament and gingiva (soft tissues) constitute the periodontium, which contributes to the stability of the tooth in the alveolar arch.

Cement is a calcified fabric that covers the root. It is an avascular tissue, and for this reason is not considered as a bone tissue.

The *gingiva* is a mucosa that surrounds the neck and covers the alveolar processes, creeps between the individual teeth to form the gingival papilla. Towards the apex of the teeth is the alveolar mucosa, which differs from the fixed gingiva in its most intense red colour. Connective tissue is the predominant component of the gingiva and consists mainly of collagen fibres (65%), fibroblasts (5%) and vessels and nerves (35%) immersed in an amorphous matrix.

The *periodontal ligament* occupies the periodontal space between the root surface and the wall of the alveolar cavity, bordering at the top with the gingiva and at the bottom with the pulp. Its function is to bind its collagen fibres (in bundles) to cement and alveolar bone; these fibres also have vessels and nerves and are therefore sensitive to pressure stresses, from which the ligament provides adequate protection of the tooth. In this tissue there are many different cells: cement blasts, osteoblasts, fibroblasts.

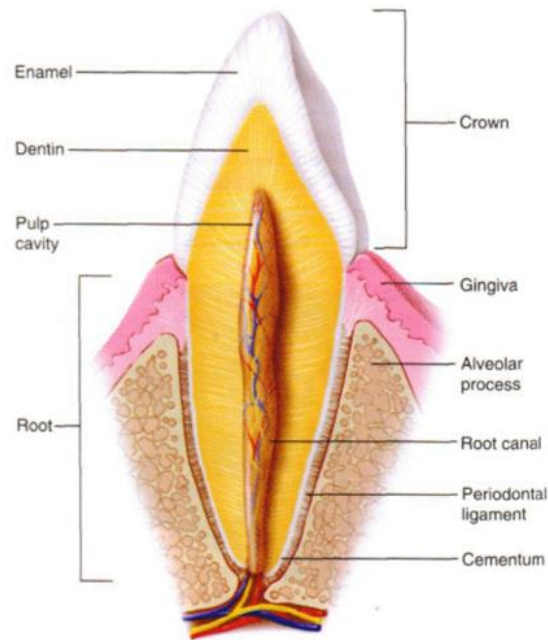


Figure 1.2: Longitudinal section of a tooth

1.2 Fibroblasts

Fibroblasts are typical (and more numerous) connective tissue cells capable of synthesizing the extracellular matrix and collagen, and play a critical role in wound healing.[1] Fibroblasts have a branched cytoplasm surrounding an elliptical, speckled nucleus having two or more nucleoli. They have dimensions of approximately 15-20 μm .

The fibers of the connective tissue are produced by fibroblasts and form the scaffolding for the extracellular matrix, also acting as connectors between the components of the matrix and the cells. Gingiva connective tissue is organized to maintain the gingival margin tightly around the tooth collar and preserve the integrity of the dentin-gingival adhesion. The collagen fibers reinforce the interdental papilla, give elasticity to the gingiva and maintain its shape.

In the gingiva, the fibrous tissue has functions of:

- support for nerves, blood vessels and lymphatics;
- separation of the epithelium from the underlying tissues;
- support for the transient cellular population;
- support for the permanent cellular population of the immune system.

Under physiological conditions, fibroblast is a long-lived quiescent cell, and generally proliferation and death are not observed.[2] In adult tissue, it plays a key role in the maintenance and homeostasis of ECM, regulating its normal turnover by controlling epithelial differentiation and inflammation. Fibroblasts synthesize the main fibrillar constituents of ECM: type I, II and IV collagen and fibronectin, and contribute to the formation of basal membranes by secretion of type IV collagen and laminin. They are also important for the synthesis of proteases, such as metalloprotease (MMPs), which are essential for matrix degradation and renewal. Fibroblasts are finally involved in the maintenance of homeostasis of neighbouring epithelia, through secretion of growth factors and direct interactions between mesenchymal and epithelial cells. [2][3]

Fibroblasts play a prominent role in normal tissue repair phenomena.[2] During these processes, the fibroblast passes from its condition as a quiescent cell to an activated phenotype expressing α -smooth-actin cushions (α -SMA), called myofibroblast, and characterized by an active proliferation and secretion of high levels of ECM protein. Activated fibroblasts release increased levels of MMPs, which favour a rapid turnover of the ECM, leading in some cases to changes in its composition, and show an increased synthesis of growth factors such as HGF, IGF, NGF, EGF, FGF2 and WNT1, which stimulate the proliferation of adjacent epithelial cells. Myofibroblasts can also modulate the immune response after tissue damage by secretion of cytokines and chemokines. [3] As a result of their activation, myofibroblasts invade the site of the tissue lesion, produce ECM which serves as a support for other cell types, and possess cytoskeletal elements that promote contraction in wound healing. [3]

1.3 Dental implant

The dental implant (also known as endosseous implant) is a surgical medical device used to functionally and aesthetically rehabilitate the loss or congenital lack of one or more teeth, allowing the support of a prosthetic replacement by direct bone support thanks to a biological process known as osseointegration; it can be inserted into both the mandible and the maxilla. [4]

Implants are not completely inserted into tissues (closed implants), as would be the case with a heart valve, but are open and interrupt the epithelial surface. Closed implants are rarely used: in them the epithelial coating is suspended at insertion and restored after the operation by means of sutures. The application of an implant is positive if the patient has enough bone tissue, extended adherent mucosa and thin epithelium. In surgical practice, the entire operation consists of two

phases which are separated in time between three and six months, to allow successful osseointegration. [5]

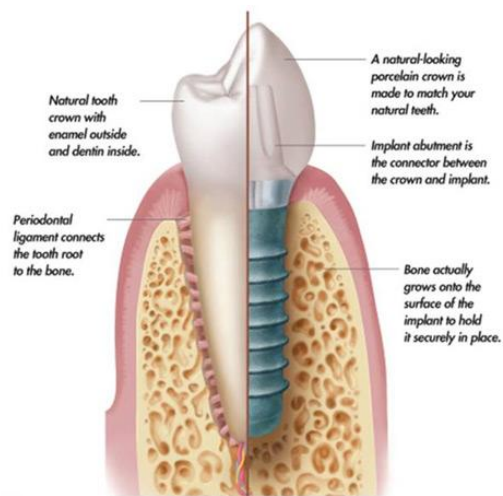


Figure 1.3: Comparison between the dental system and implant system

A dental implant consists of three components: [5]

- implant body
- abutment
- crown

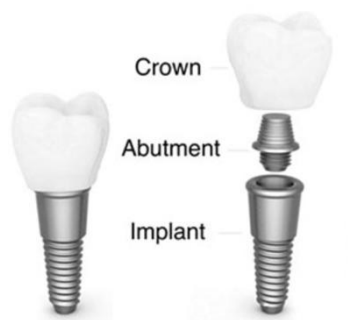


Figure 1.4: Dental implant components

The classification of plants includes different types:[5]

Subperiosteal implants: a metal structure is surgically placed between the bone surface and the periosteum, then immediately above the bone; the pillars of the implant pass through the mucous membrane covering it in some places. These implants are rarely used because of their

shape, which is not very similar to natural roots. Good osseointegration cannot be achieved and have high failure rates.

Endosseous implants: the implant is inserted into the bone in a direct way; while closed implants, placed under the periosteum, cannot communicate with the oral cavity, open implants have a pillar with this function. Most endosseous implants are of the latter type; there is a subtype of endosseous implants intended to remain below an intact epithelial layer for several months (healing phase) and which is only exposed externally at a later time. These implants are relatively common, due to the simpler surgical techniques and the possibility of applying a new implant in case of failure.

Subperiosteal endosseous implants: these are a combination of the two previous types; a part is above the bone, a part is inside it.

Transosseous implants: these are specific to the mandible and pass through it vertically.

Transdental implants: they are also called endodontic implants because they stabilize the teeth in which they are placed: they have a sort of "biological collar" for the anchoring between the seal of separation with the oral cavity and the periodontium of the natural tooth.

Intramucosal implants: they are inserted into the covering mucosa by fixation to a prosthetic base; since they do not perforate the covering epithelium and do not remain permanently in the implant seat, they are better suited to fall within the classical prosthetic field than in the implant one.

1.4 Implant success and durability

The implants used today have made it possible to overcome the problem of rejection because they have the capacity to integrate with natural tissues (osseointegration).

The success of an implant depends on the satisfaction of different conditions:[6]

- the implant is functional under load, i. e. does not cause pain and is clinically stable;
- the periodontium is clinically stable and not bleeding;
- phonetic, aesthetic and chewing functions improve;
- no increase in bone destruction is observed;
- there is no radiotransparency (limited attenuation capacity of the X-rays);
- the patient's health is not altered.

In addition, clinical success in implantology depends on a number of closely interlinked factors, such as:

- the type of implant (form, surface structure);
- the nature of the materials used;
- the interactions between bone tissue and implantation.

Implant failure factors, which are not related to the patient's sex and are not very age-dependent, may be:

- inappropriate choice of implant type (shape and material);
- incorrect seat for the system, without observing the proper contraindications;
- incorrect surgical technique, with intraoperative consequences and post-operative;
- no immobilization or infection after the operation;
- excessive load or insufficient load, both not favourable to osseointegration;
- inappropriate amount or quality of bone (e. g. osteoporosis);
- health complications in the patient and poor oral hygiene.

The main symptoms that appear as a result of implant failure are: mobility (already during the first year), infection formation, compression pain, bone destruction, osteitis, sensitivity disorders, uncovered implant parts, maxillary sinusitis.[6]

Immediate failure is related to the rapid destruction of bone and graft contact, which immediately creates implant mobility. The late failure, on the other hand, is linked to the advancement of bone resorption, to the depth of the insertion into the bone, to the inadequacy of the tissue or the starting surface, and causes mobility only after a few years. Ideally, there should be no immediate or late mobility, and prevention from infections of the environment around the implant (peri-

implantitis) is desirable. Unfortunately, the latter are more frequent in rough superficial implants, which are more common because of their osteoconductive properties. [6]

1.5 Peri-implant and periodontal soft tissue

Periodontium is the tooth support apparatus consisting of: [7]

- Gingiva;
- paradoxical ligament;
- root cement;
- alveolar bone.

The tissues surrounding the dental implants include peri-implant mucosa and peri-implant bone. From a clinical point of view, peri-implant tissues and periodontal tissues around teeth can have many clinical features in common, but there are marked structural differences between the two types of tissues. The natural tooth has a mechanical anchorage to adjacent gingival tissues and alveolar bone using supracrestal collagen fibres and periodontal ligament. Fibres are inserted into the root cement of the tooth and into the alveolar bone. There is no root cement or periodontal ligament around the dental implants and the peri-implant bone and peri-implant mucous membrane form a direct contact with the implant. The integration of hard and soft tissue with the implant is the result of a wound healing process that lasts several weeks.[7] The interface between mucosa and implant is an area of fundamental importance for the health of the implant itself, and in this area the local immune response develops to counteract bacterial attacks and preserve osseointegration.

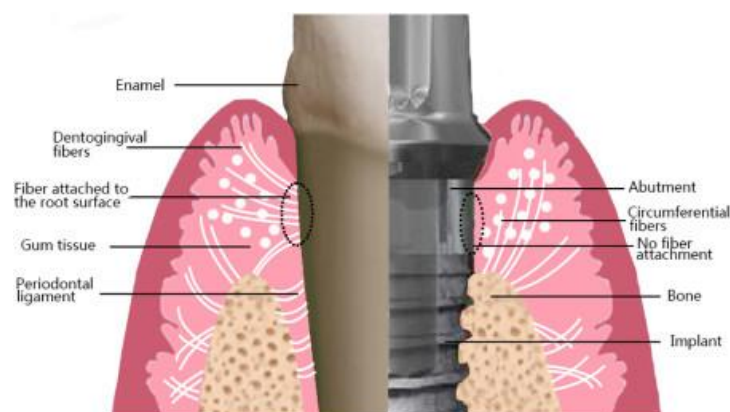


Figure 1.5: Periodontal and peri-implant and soft tissue

The internal interface between soft tissue and tooth or implant is coronally represented by junctional epithelium with a width of about 2 mm and apically by supracrestal connective tissue with a width of about 1-1.5 mm. The integrity of this mucous seal (epithelial and connective tissue) provides a barrier to bacterial attacks against deep periodontal tissue.

The implant unit is without periodontal ligament, periodontal vascular plexus, neurosensory system and cement, which surround the natural elements. The union of the implant with collagen fibers is prevented by the absence of cement on the implant itself. In the natural tooth, the connective fibers have a predominantly horizontal pattern and are inserted into the root cement. In the implant they originate from the periosteum of the bone crest and are parallel to the implant surface. At the supracrestal area, the connective tissue is richer in collagen fibers, but has a smaller cellular population represented by fibroblasts and a lower vascularization than that of natural teeth, thus assuming the characteristics of a scar tissue. In addition, the connective material appears to be strictly adherent to the thin layer of titanium oxide covering the implant surface. Around the implant, there are also circular connective fibers. *Fibroblasts* present at this level have the function of maintaining and, if necessary, re-establishing cohesion between the connective tissue and the implant surface.[8]

The response to the accumulation of bacterial plaque is quite similar in periodontal soft tissues and peri-implant tissues, but the latter have less resistance to inflammatory processes caused by bacterial plaque.

1.6 Peri-implant mucositis and peri-implantitis

The long-term success of implants can be seriously compromised by bacterial infections leading to peri-implant diseases, i. e. diseases affecting soft and hard tissue, supportive of implants.[9] From a clinical point of view, inflammatory processes affecting peri-implant tissues occur in two forms: *peri-implant mucositis* and *peri-implantitis*. It was reported in 5–11 year observations that peri-implant mucositis affects 40–90% of implants in 80% of subjects, while around 20% of implants develop peri-implantitis. The first, which affects soft tissue, can also be solved completely, allowing total healing. The second, affects both tissues and is a more serious infection, which causes reabsorption (Fig. 1.7).



Figure 1. 6: Healthy dental implant (left) vs dental implant susceptible to infection (right)

Peri-implantitis is mainly due to bacteria that accumulate in the mouth and on the surface of the prosthetic elements. If bacteria reach the implant surface, they damage the tissue near the implant itself. Peri-implantitis is, however, the last act of a series of events that can and must be intercepted much earlier. The bacteria, once organized in colonies, give rise to bacterial plaque. If these are not promptly removed, due to the production of their metabolites they cause inflammation of the gingiva close to the implant. This inflammation is called peri-implant mucositis. If etiological factors are removed promptly, the tissues can heal without any consequences. However, if the inflammatory state persists over time, the situation will gradually deteriorate with the evolution from peri-implant mucositis to peri-implantitis. Peri-implantitis is also an inflammatory process that affects peri-implant tissues characterized by a progressive loss of bone tissue; if not treated in its initial phases, it leads irreparably to the loss of the implant. As a result, good oral hygiene is essential to maintain peri-implant tissues in good health. [10]

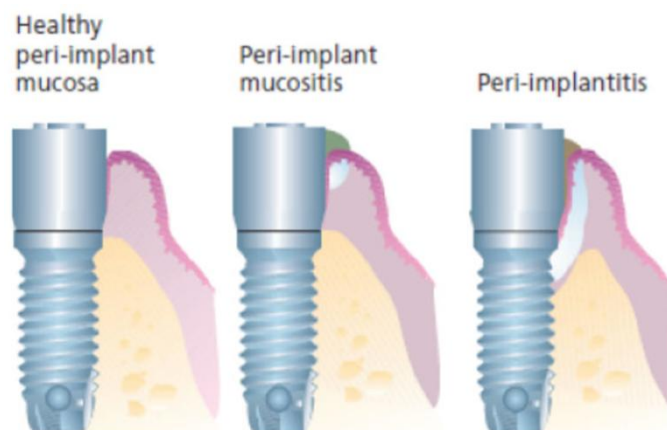


Figure 1.7: Healthy peri-implant mucosa (a); inflammation peri-implant mucosa (b); inflammation peri-implant mucosa and progressive loss of bone (c)

Natural teeth are able to fight periodontal disease for many years, while implants are not able to do the same, and therefore their survival in mouths of patients suffering from periodontitis is absolutely precarious. Particular attention is therefore paid to the design of the collar, which must be such as to minimize the accumulation of plaque.

1.7 Oral cavity bacteria

Bacteria constitute a large domain of prokaryotic microorganisms. A prokaryote is a unicellular organism that lacks a membrane-bound nucleus, mitochondria, or any other membrane-bound organelle. Their DNA is generally dispersed in the cytoplasm in an internal cell region called the nucleoid. Prokaryotes cells have a very simple internal structure compared to the eukaryotes. The cell membrane is surrounded by a rigid structure: a cellular wall, formed by a substance consisting of complex sugars and bound to other molecules, which serves to protect and shape the cell. Typically a few micrometres in length, bacteria have a number of shapes, ranging from spheres to rods and spirals. [11]

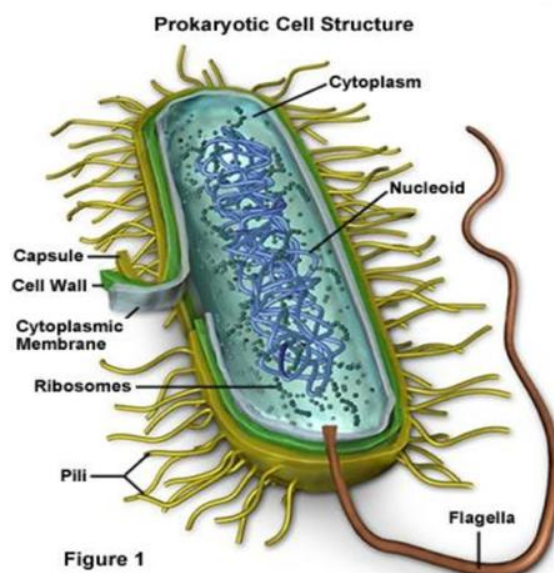


Figure 1.8: Bacterium structure

According to shape, the bacteria can be classified in: [11]

- *Bacilli*: stick-shaped. It includes two orders, Bacillales and Lactobacillales. They are gram-positive bacteria.
- *Coccus* (plural cocci): spherical, ovoid, or generally round shape. If they are arranged in the grape-like shape, they are called Staphylococci (e.g. *Staphylococcus aureus*).
- *Vibrio*: curved-rod shape (comma shape). They are Gram-negative bacteria.
- *Spirillum*: spiral-shaped. They are Gram-negative bacteria.

Bacteria can also be classified as Gram positive and Gram negative, based on how they respond to Gram colouring.[12]

Gram-positive bacteria have a very thick cell wall rich in a polymer called peptidoglycan. In these bacteria peptidoglycan makes up about 90% of the cell wall. In Gram colouring, the application of the colorant makes them acquire the purple colour. Gram positive bacteria are some streptococci, staphylococci, pneumococci.

Gram-negative bacteria have a thinner cell wall and contain only 15/20% peptidoglycan, they are red after staining. Negative bacterial infections are less frequent than those of positive bacteria such as streptococci and staphylococci; however, in general, Gram-negative bacteria are much more damaging and dangerous, as well as involved in a myriad of different disorders and diseases.

Gram-positive aerobic bacteria were observed on dental implant surfaces surrounded by healthy oral environment.[13] *Staphylococcus aureus* is a Gram positive bacterium belonging to the bunch genus, with a diameter of 0.8-1.5 μm , which is typically found in irregular clusters (from Greek $\sigma\tau\alpha\upsilon\upsilon\lambda\acute{\eta}$ = bunch), is asporigial, immobile and can be either capulated or not. It is an optional anaerobic, capable of breathing and also fermenting glucose with lactic acid production; it is catalase positive and catalyses the splitting of H_2O_2 into $\text{H}_2\text{O} + \text{O}_2$. It shows remarkable resistance to high NaCl concentrations (7.5%) which is able to inhibit most other bacteria (these ions are in fact contained in saliva with the purpose of inhibiting bacterial activity). It is called "aureus" because it generally produces a golden yellow pigment, but the pigmentation may vary

from light yellow to dark orange. It multiplies in aerobiosis at 37°C, giving rise to typical colonies: pigmented, smooth, shiny, roundish with net margins.[14]

1.8 Osseointegration

The term osseointegration was coined in the late 1960s by Per-Ingvar Brånemark, Swedish professor of applied biotechnology. This term is used in dentistry and medicine to define the intimate bond between a bone and an artificial implant, without apparent connective tissue. It is defined as intimate union when the space and relative movements between bone and implant do not exceed 100 microns. Osseointegration is also considered a measure of implant stability in the implant site. This can be achieved in two different phases, defined as primary and secondary respectively. [6]

The *primary stability* of an implant derives mainly from the mechanical interaction of the implant itself with the bone.

The *secondary stability* is the biological stability achieved through bone regeneration and remodeling.

Primary stability is a prerequisite for secondary stability and depends on implant shape, bone quality and implant bed preparation. It decreases gradually in the bone remodeling process. The transition from primary to secondary stability is dictated by the advancement of the healing process. A stable implant has "limited" micromovements between bone and implant (not exceed 100 microns); this allows tissue growth around the implant itself according to a process similar to healing a bone fracture. Excessive implant movement leads to the formation of fibrous connective tissue between bone and implant. The surgical intervention required to introduce the implant and produce primary stability of the implant itself leads to haemorrhage from the surrounding bone and soft tissue, resulting in haematoma formation. From this start a series of biological processes at the base of osseointegration. The implant immediately comes into contact with the blood and this triggers a series of biological processes such as: protein deposition, platelet activation and coagulation, inflammation and signaling and lastly tissue formation. These processes represent the

host's response to injury and implant introduction and are influenced by the chemical-physical and topographical characteristics of the implant surface. [15]

During surgery, blood vessels are damaged, causing bleeding and coagulation. Platelets play a major role in clot formation. Their activation leads to a change in their shape and release into the environment of different growth factors such as PDGF (platelet-derived growth factor) and TGF- β (transforming growth factor beta), and vasoactive factors. Several in vivo and in vitro studies have shown that these growth factors have an important effect on migration and proliferation of different cell types.[16] Some authors have shown that these growth factors are mitogenic and chemotactic factors for fibroblasts. [17]

According to current knowledge, the intimate bond between a bone and an artificial implant only occurs when the implant is made of titanium, but also metal materials with a suitable micromorphology and without proteins could induce osseointegration. The speed of the osseointegration process and its quantity vary according to the type of implant surface, which may have a geometry that attracts osteoblast cells. A smooth surface is less suitable for this purpose, so special treatments can be used to obtain a rough surface; the most common are acid etching or sandblasting. Recent studies have shown that if the implant has a spongy surface, the process is considerably faster and more intimate. On the other hand, a spongy or highly roughened surface is much more susceptible to bacterial colonisation which can easily lead to implant loss.[18]

2. Titanium and Titanium alloys

2.1 Biomaterial

Biomaterial is defined as a material designed to interface with biological systems in order to evaluate, support or replace any tissue, organ or function of the body.[19] Biomaterials are used in intimate contact with the body and it is fundamental that the implanted material does not cause any noxious effect. Biocompatibility plays a key role in this context.[20]

Biocompatibility can be defined as “the ability of a material to perform with an appropriate host response in a specific application” as proposed by Williams in 1987.[21]

In addition to the mass properties of the material it is very important to evaluate the biocompatibility of the surface of an implant, because it is the part directly in contact with the host organism. Implants can be classified according to the interaction between the material and the surrounding tissues as shown below:[22]

- *Incompatible*: Release of substances in toxic concentrations that lead to inharmonious effects with the living organism that may result in a rejection of the implant.
- *Biotolerant*: Release of substances but not in toxic concentrations that may lead to an encapsulation within connective tissue.
- *Bioinert*: Release of substances but not in toxic concentrations that may lead to an encapsulation within connective tissue.
- *Bioactive*: Positive interaction with differentiation of tissue that leads to a close adhesion and interconnection along the interface of implant and tissue.

There are three categories of materials used for biomedical implants: metals, ceramics, polymers.
[23]

Polymeric materials are generally organic substances (but there are also important inorganic polymers) consisting of large molecules (macromolecules) formed by the repetition of identical or different units called monomers. The structure of polymers can vary significantly and they are characterised by poor electrical conduction, low density and low softening temperatures. The mechanical properties are extremely variable depending on the nature of the constituents and the type of polymer structure. Polymers make up about 45% of biomaterials and their typical applications range from orthopaedics, cardiovascular prostheses to the production of whole artificial organs.

Ceramic materials can be obtained by combining a wide range of raw materials and can exist in a wide variety of shapes, both crystalline and glassy (or amorphous). The atomic structure of ceramic materials (nature of the chemical bond and microstructure) gives them the properties of excellent resistance to heat and attack by chemical agents, as well as electrical and thermal isolation and good resistance to compression loads. Unfortunately, it is also the cause of a mechanical behaviour characterized by fragility: the crystalline structure of ceramic materials does not allow the relative movement of atoms, so when the material is deformed beyond a certain limit, it suffers a fragile fracture.

Metals are widely used as materials for biomedical devices. The applications are varied and range from equipment components to whole dentures or parts thereof. Most are used in the manufacture of surgical instruments, orthopaedic and dental prostheses. Metallic materials have important characteristics such as:

- High elastic modulus (100÷200 GPa) and high yield strength (300÷1000 MPa): thus make it possible to build structures capable of supporting high loads without large elastic deformations or permanent plastic deformations.
- Good ductility; when the applied stress exceeds the yield strength, the structure deforms plastically rather than brittlely breaking. This allows to replacing the deformed component before it breaks.
- High resistance to mechanical fatigue, which makes them suitable for all applications where load cycles are expected

The first metal specifically developed for human use was the Sherman Vanadium Steel (1912, Vanadium Steel), used to manufacture plates and screws used in bone fractures. Other metals used over time are: iron, chromium, cobalt, nickel, titanium, tantalum, molybdenum, and tungsten. Some of them have been abandoned due to toxicity problems. The biocompatibility of

metals is linked to their corrosion in biological environment: biological fluids have a high corrosive power against metals.

2.2 Titanium

Titanium is located in the fourth group of the periodic table with atomic number 22, it has excellent properties from the engineering point of view; it exhibits low density, high strength (resistant as steel and twice as resistant as aluminium), low modulus of elasticity, low thermal conductivity, low thermal expansion, excellent corrosion resistance, ease of processing, biocompatibility, extremely short radioactive halving period (which allows its use in nuclear systems), is not magnetic and is capable of sustaining extreme temperatures (thanks to its high melting point). Furthermore, titanium is immune to the corrosive attack of saltwater or marine environments and exhibits exceptional resistance to a wide range of acids, alkalis, natural waters and industrial chemicals; finally, it offers great resistance to erosion attacks (it is at least twenty times more resistant to erosion than copper-nickel alloys), cavitation and impacts.[24]

Titanium has an allotropic behaviour: it exists in several crystalline forms. Pure titanium crystallizes at low temperatures (room temperature) in a compact hexagonal structure (H. C. P., Hexagonal Closed Pack), called the α phase. Above the β -transus temperature (approximately 882°C), the microstructure of titanium transforms into a centered body cubic structure (B. C. C., Body Centered Cubic), called β phase. The great variety of properties obtainable with titanium alloys is due to the existence of these two different crystalline structures, which allow to obtain different microstructures depending on the alloy elements present and the thermal treatments carried out. [25][26][27][28]

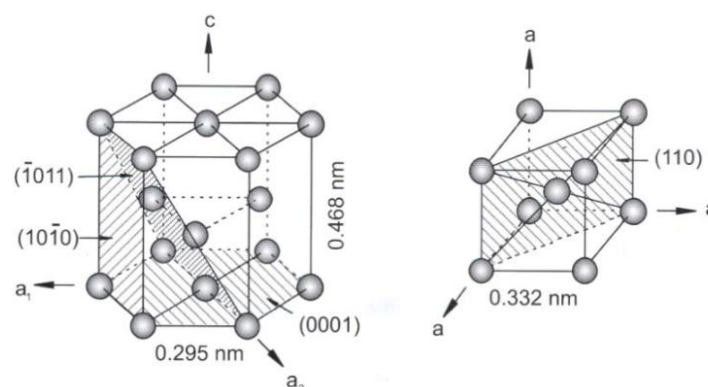


Figure 2.1: Crystal structure of hcp α and bcc β phase

This metal has a boiling temperature of 3285°C and a high melting point (1660°C). The addition of alloy elements can change the melting temperature and transformation temperature $\alpha \leftrightarrow \beta$.

Titanium is characterised by a low density (4.54 g/cm³), approximately 56% of that of steel; for the same weight, therefore, titanium occupies twice as much volume as steel, with the former it is possible to make lighter components. Therefore, titanium is as strong as steel, but 56% lighter, and 60% heavier than aluminium, but twice as strong. The density is influenced by the quantity and density of the alloy elements. Beta alloys are generally the heaviest because they contain alloy elements, such as molybdenum, which have a high density. The combination of low linear density and high strength produces particularly favourable strength/weight ratios, superior to almost all other metals.[25][26][27][28]

Titanium has very low thermal conductivity and thermal expansion coefficients of approximately 26 W/mK and $6.9 \times 10^{-6} \text{ }^\circ\text{C}^{-1}$, respectively, which are far lower than aluminium; also exhibits very high reactivity with most other elements. These characteristics require the use of appropriate techniques and precautions in processing both for melting and plastic deformation and for mechanical processing. Titanium has a thermal expansion coefficient significantly lower than that of ferrous alloys; this property allows it to be much more compatible with ceramic materials or glass than other metals, especially when metal/glass or metal/ceramic seals are involved. [24]

Titanium has an elasticity modulus of 106 GPa, about half that of steel; this low modulus means excellent flexibility, which is the basic property for its use in dental devices (supports, etc.). The excellent biocompatibility of titanium provides an additional reason for the rapid expansion of titanium for use in body prostheses.[24]

The environmental resistance of titanium depends above all on a very thin, tough and highly protective surface oxide film (mainly TiO₂), very stable above a certain pH, potential and temperature range, whose formation is particularly favoured when the oxidising character of the environment increases; for this reason, titanium generally resists slightly reducing, neutral and highly oxidizing environments up to reasonably high temperatures. Titanium develops very stable surface oxides with high integrity, tenacity and good adhesion. Surface oxide on titanium, if scratched or damaged, can immediately be reconstructed in the presence of air or water.[24]

2.3 Titanium alloy

As previously mentioned, at room temperature titanium has a hexagonal crystalline structure with maximum packaging (α); at about 882°C the α phase transforms into a centered body cubic structure (β), which is stable up to the melting point, which varies between about 1650°C and 1700°C. The temperature of this allotropic transformation is a function of the content of alloy elements. Alloy elements are classified according to their influence on the transition temperature between phases α and β (i. e. β -transus temperature, defined as the lowest equilibrium temperature at which only phase β is present in the material). Three types of elements can be distinguished:[25][26][27][29]

- neutral elements: elements which have no influence on the transition temperature between the two phases, but which increase the resistance of the α phase (Tin and Zirconium).
- α stabilizing elements: increase the transition temperature between α and β phases, extending the stability range of the α phase at higher temperatures. These include aluminium, the most important and used, oxygen, carbon, nitrogen, gallium and germanium. Aluminium, together with the tin and zirconium mentioned above among the elements, is soluble in both α and β phases and therefore tends to spread evenly between them, increasing creep resistance of the α phase.
- β -stabilizing elements: they reduce the transition temperature between the two phases, extending the stability range of the β phase at lower temperatures. They are subdivided into β -isomorphous elements, such as molybdenum, vanadium, tantalum and niobium, which are more important for their greater solubility in titanium, and β -eutectoid elements, such as iron, manganese, chromium and cobalt, nickel, copper, silicon and hydrogen, which can lead to the formation of intermetallic compounds even at low percentages and which are therefore mainly used in the presence of β -isomorphous elements to limit this phenomenon. In particular, silicon is used in some alloys to improve creep resistance, iron, chromium and manganese are used to increase hardenability and sensitivity to thermal treatments of the alloy, while nickel, molybdenum and palladium increase resistance to corrosion.

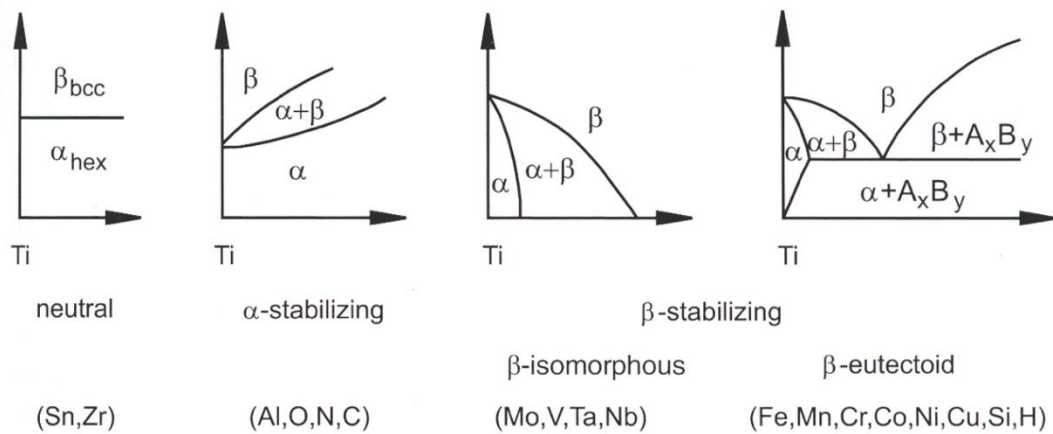


Figure 9.2: Influence of alloying elements on phase diagram of Ti alloy

The classification of titanium alloys is based on alloy elements, distinguishing between three main groups:

- alloys α : these include alloys containing only α stabilising or neutral elements. If small percentages of β stabilizing elements are contained in the alloy, this is referred to as near α ;
- alloys $\alpha+\beta$: contain a percentage of phase β at room temperature which fluctuates approximately between 5 and 50%, due to the presence of α and β alloy stabilisers. These are the most commonly used alloys;
- alloys β : alloys containing β phase only (single-phase β alloys) or containing α and β phase at room temperature, but in which martensitic structure formation does not occur even after tempering (metastable β alloys).

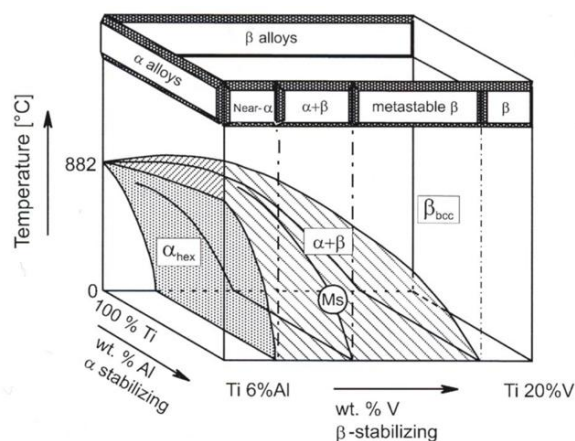


Figure 2.10: Schematic Phase diagram to classify Ti alloy

In addition to alloys there is also unalloyed titanium (titanium CP or commercially pure), in which other elements are present in very small percentages and considered as impurities.[29][28] There are 4 types of titanium CP for biomedical applications depending on the impurities present: these contain 99.01% to 99.5% titanium, and small quantities of iron, carbon, hydrogen, nitrogen and oxygen. These elements are normally present in residual form and do not have a significant effect on mechanical properties; hence CP titanium is an alloy of titanium and interstitial elements.

	% composition			
	Grade 1	Grade 2	Grade 3	Grade 4
N, max	0.03	0.03	0.05	0.05
C, max	0.10	0.10	0.10	0.10
H, max	0.015	0.015	0.015	0.015
Fe, max	0.20	0.30	0.30	0.50
O, max	0.18	0.25	0.35	0.40

Table 2.1: Chemical composition of titanium CP

Usually, unalloyed titanium is used in applications where excellent corrosion resistance is desired and where high strength is not a determining factor. In addition, in CP titanium, oxygen acts as a controlled strengthening agent: resistance increases if it increases the amount of oxygen within a controlled range, because too much oxygen makes the material more fragile.

Material	Modulus (GPa)	Ultimate Tensile Strength (MPa)	Yield Strength (MPa)	Elongation (%)	Density (g/cc)	Type of Alloy
Cp Ti grade I	102	240	170	24	4.5	α
Cp Ti grade II	102	345	275	20	4.5	α
Cp Ti grade III	102	450	380	18	4.5	α
Cp Ti grade IV	104	550	483	15	4.5	α

Table 2.2: Mechanical properties of commercially pure titanium

Titanium alloys have found great use in biomedical applications due to their excellent chemical, mechanical and biocompatibility properties. In particular, the low elastic modulus avoids stress

shielding after implantation. Titanium alloys are also used as bone replacements due to their excellent corrosion resistance and show high fatigue strength compared to other metal materials. [29] Beta titanium alloy containing non-toxic elements such as Mo, Zr, Ta, Nb show low modulus of elasticity, high corrosion resistance and improve the response of biological tissues. Due to their excellent biomedical properties, these titanium alloys can be used to replace TiAl4Va alloy, which is currently considered the most important biomedical alloy.[30]

In conclusion, the use of titanium alloys has proven to solve some of the major problems associated with implant failure (Fig. 2.4).

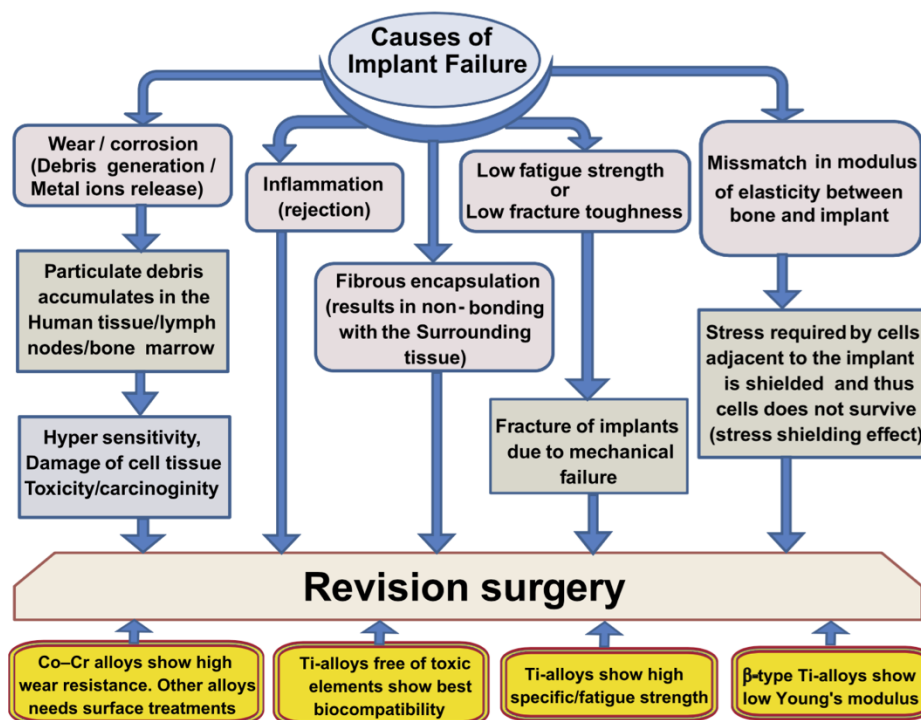


Figure 2.11: Various causes for failure of implants that leads to revision surgery, footed with a proposed system for better performance.

2.4 Ti15Mo

Molybdenum is a β -stabilizing elements and therefore allows to lower the β -transus temperature; it also allows to improve the strength, corrosion resistance, high temperature performances and formability of Ti alloy. Molybdenum is an element with non-toxic and non-allergic characteristics,

which makes it possible to obtain titanium alloys with low modulus of elasticity and high strength for biomaterials.[31]

Ti15Mo is a titanium alloy composed of 15% molybdenum and therefore belongs to the beta titanium alloys, in particular it is a monophasic β alloy. Ti15Mo is a material that has recently found use in the biomedical sector, it was originally developed to improve corrosion resistance. The following table lists the composition limits for Ti-15Mo, specified by a standard (Table 2.3). Important physical properties are also summarized in Table 2.4. [32]

Element	Composition [wt. %]
Ni	max 0.05
C	max 0.1
H	max 0.015
Fe	max 0.1
O	max 0.2
Mo	14.0-16.0
Ti	Balance

Table 2.3: Composition limits for Ti-15Mo alloy

Density [mg/cm^3]	4.96
Modulus of Elasticity in Tension [GPa]	78 (β) 105 ($\alpha + \beta$)
Electrical Resistivity at 31 °C [$\mu\Omega \text{mm}^{-1}$]	800
Mean Coefficient of Thermal Expansion from 50–600 °C [$10^{-6}/^\circ\text{C}$]	8.5
Thermal Conductivity at 31 °C [$\text{cal}/\text{cm s}^\circ\text{C}$]	0.03

Table2. 4: Physical properties of Ti-15Mo alloy

The amount of Mo inside titanium influences the phase composition: in fact for Mo less than 10% there are both α and β phases, while for content greater than 10% there is only the β phase. It is therefore possible to stabilize the β phase at room temperature by increasing the Mo content. In addition, for Mo content greater than 10%, a smaller and more equiaxial beta grain structure compared to lower concentrations can be observed.[31]

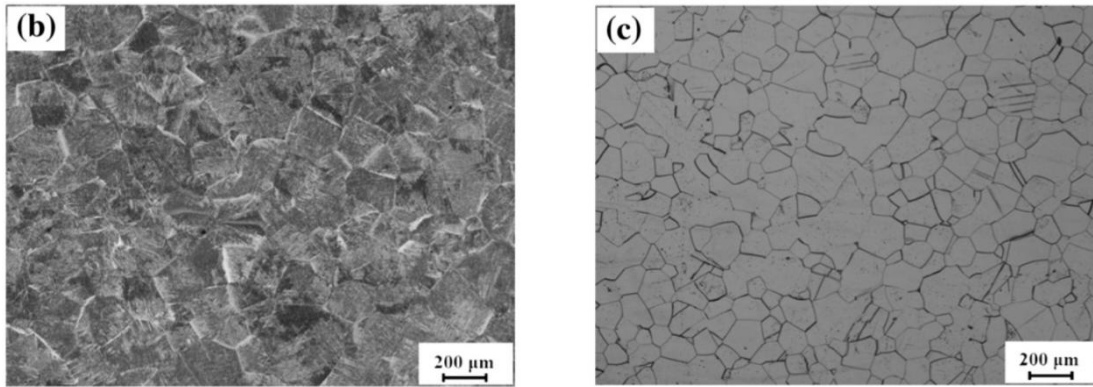


Figure 2.12 : Microstructures of Ti4Mo (b) and Ti15Mo (c)

Mo content also influences the strength and plasticity at room temperature: these factors increase as the Mo content increases and decrease as it decreases. In conclusion, an increase in Mo content affects grain size and moreover, smaller grains improve resistance and plasticity at room temperature.[31]

In general, grain size plays an important role in titanium alloys, in fact the microstructure drastically influences the properties of titanium alloys, and can be modified by appropriately choosing the thermal treatments and mechanical processes that the alloy undergoes. The microstructure of titanium alloys is essentially described by the size, shape and spatial arrangement of the α and β phases. The two borderline microstructural situations are the lamellar microstructure, generated by rapid cooling from the β phase stability field, and the equiaxial microstructure, resulting from a recrystallization process; both types of microstructure may have a fine or gross arrangement of the two phases. [25][26][27]

Although the correlation between microstructure and heat aging treatments in Ti-Mo is not yet fully described in the literature, some authors have shown that aging heat treatments on Ti15Mo can induce α phase precipitation in the β matrix: both inside and in the grain boundaries.[23]

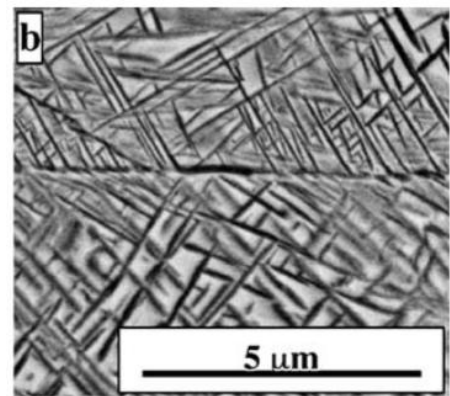


Figure 2.13: Alpha precipitations in beta grains

Thanks to alpha precipitations, it is possible to strengthen the Ti15Mo. Ageing can also produce an undesirable ω phase. This phase significantly increases the mechanical strength of the alloy, but also causes great fragility. In addition, the presence of phase ω in a β matrix can act as a nucleation substrate for the formation of fine and uniform distributed α -phase in the beta matrix.[33]

2.5 Electron Beam Welding (EBW)

In the biomedical sector, electronic beam welding is used to create controlled surface structuring on prosthetic materials. The surface of the prosthesis is treated in the area that will come into contact with bones and tissues. Indeed, in this area the titanium denture should have an appropriate roughness surface to encourage cellular adhesion. EBW obtains this roughness through a particular surface treatment: high-speed electrons are concentrated in a thin beam, directed towards the workpiece, the contact between the beam and the workpiece generates heat that melts the material. Thanks to this technique, it is possible to create a microstructure on the surface of titanium.[34]

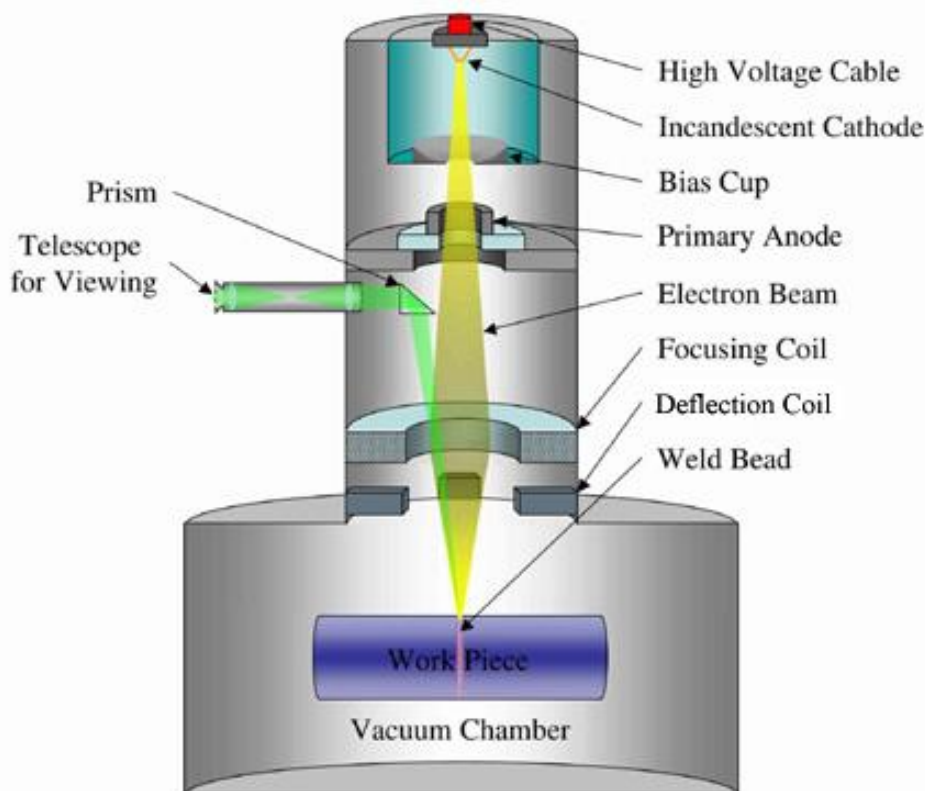


Figure 2.14 Electron Beam Welding

EBW is a thermoelectric process in which very high temperatures and density of thermal energy are reached. Free electrons are produced by heating the cathode (mainly made of tungsten) and are accelerated towards the anode by a potential difference. The tension between anode and cathode is called accelerating voltage and affects the velocity of electrons and the thermal energy that develops as a result of electronic bombardment. The electrons reach a speed between 5000 and 200000 Km/sec. The electron beam passes through the anode hole and is then focused by an electromagnetic lens that reduces its diameter. The beam thus obtained strikes the material that melts instantly. The heat is caused by electrons that stop on the piece: 99% of the kinetic energy lost by electrons is transformed into heat and the remaining 1% into X-rays (this makes it necessary to use screens to protect the operator). The cannon is placed in a vacuum chamber and moves vertically; the beam remains stationary and the workpiece is moved at the desired speed under the electron beam (feed motor).[35] Thanks to the high density that transmits to the material, the electron beam causes melting and evaporation of the material, forming a cavity called keyhole.

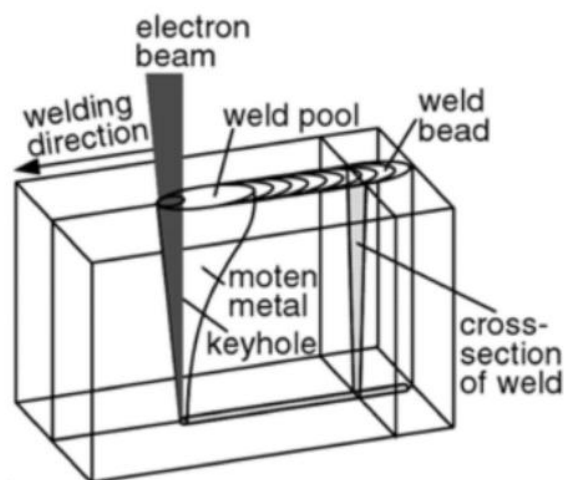


Figure 2.15: Microgrooves formation following electron beam passage on titanium

The beam power is given by the following equation:[32]

$$P_b = U_A \cdot I_B$$

where U_A indicates the acceleration voltage and I_B the beam current. Typically for an acceleration voltage of 150 kV the electrons reach a velocity of $2 \cdot 10^8$ m/s.

3. Surface micro/nano structuring

3.1 In vivo cell-matrix interaction

In vivo, the cell recognizes the environment that surrounds it and interacts with it. The microenvironment, in which the cells are immersed, is represented by the Extra-Cellular Matrix (ECM): a complex entity, composed of numerous proteins that perform structural and signal functions. The interaction between cell and ECM promotes adhesion and triggers a cascade of intracellular signals that allow growth, proliferation and differentiation. The ECM represents the mechanical scaffolding for tissue architecture and plays a key role in regulating some of the most important cellular functions. Every tissue of the human body is composed of a distinct population of specialized cells, programmed to perform tissue specific functions, and a distinct extracellular matrix (ECM) responsible for stability and biomechanical properties of the tissue.[36]

3.1.1 Extracellular matrix structure and function (ECM)

The extra-cellular matrix (ECM) represents the environment outside the cells in contact with the cell membrane. The ECM represents the supporting structure that surrounds cells and promotes cell interaction with the surrounding world. The cell and the ECM have in fact a one-to-one relationship; they influence each other. ECM includes a variety of locally secreted proteins and polysaccharides, which are aggregated in a compactly organised grid connected to the surface of the cell that produced it. The ECM is composed of a complex structure formed by fibrous proteins and proteoglycans. Proteins are divided into proteins with structural function such as elastin and collagen and proteins with adhesive function, such as fibrillin, fibronectin and laminin. The molecules of proteoglycans form a gelatinous and strongly hydrated substance in the connective tissues, in which fibrous proteins are immersed.

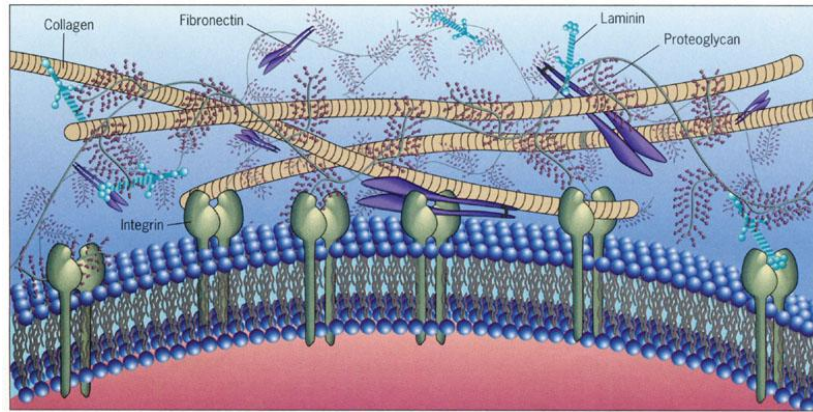


Figure 3.16: Extracellular matrix composition

The components of the ECM are specific to the considered tissue, each cell type is surrounded by an ECM with a variety of protein. It is therefore very important to reproduce in vitro an environment as similar as possible to the ECM in order to communicate with cells, influencing their development, migration, proliferation and metabolic function.

3.1.2 Cell membrane structure and function

The cell membrane separates the cell from the extracellular environment and at the same time regulates exchanges with it. The structure of the cell membrane consists of a phospholipid bilayer: phospholipid molecules arranged with the hydrophobic tails oriented towards the inside and the hydrophilic heads towards the outside. It is also composed of whole membrane proteins, which form channels that regulate the passage of ions and act as receptors. Peripheral proteins anchor the cytoskeleton and accelerate some chemical reactions. Finally, there are, membrane carbohydrates that lubricate and protect the cell membrane and can function as receptors.

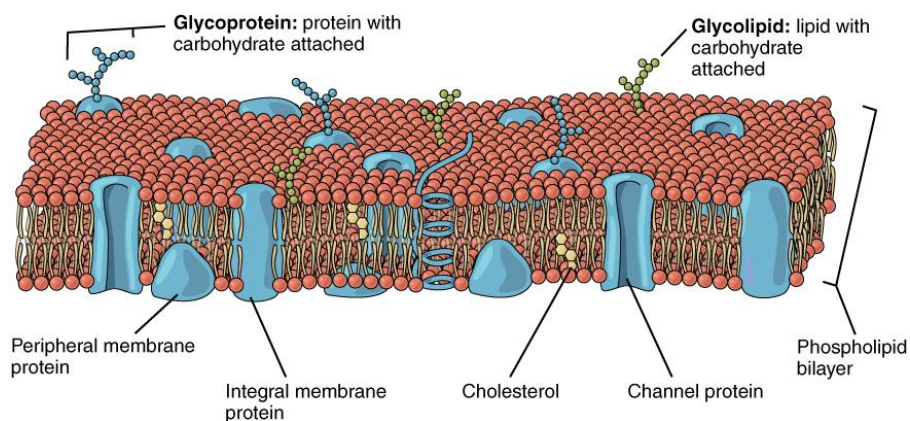


Figure 3.17: Cell membrane structure model

3.1.3 Cell-ECM adhesion

The extracellular matrix (ECM) may influence cell cytoskeleton organization, cell survival and cell proliferation. Most cells have to stick to ECM to grow and proliferate and in many cases also to survive. This phenomenon is called *anchorage dependence*. Cellular adhesion is an indispensable process for the regulation of all important cellular functions, and it involves transmembrane adhesion proteins that act as matrix receptors and bind it to the cytoskeleton.[37]

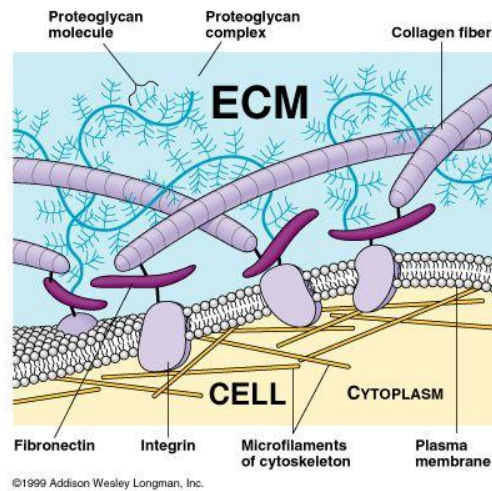


Figure 3.18: Cell-ECM contact mediated by integrins

Cell contacts with adhesive ECM proteins are mediated by a variety of cell surface molecules including integrins, lectins, and membrane-intercalated proteoglycans such as syndecans and glypicans. [36] The main receptors for binding to ECM proteins are integrins.

Integrins are a family of heterodimers transmembrane glycoproteins, composed of two subunits α and β , not covalently bound together. They play a role in the connection of the cell to the extracellular matrix and in the transduction of the signal from the ECM to the cell.[37] These can bind to different proteins of the ECM, such as fibronectin, laminin and collagen (Fig. 3.4).

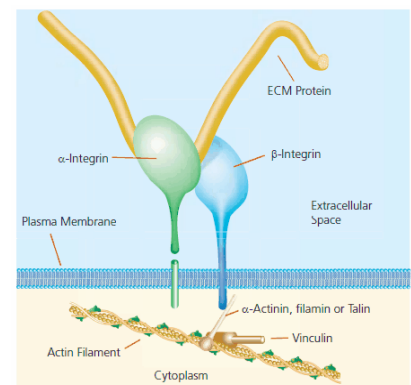


Figure 3.19: Integrin structure

The connection is made between the head of the molecule of integrin that binds to an ECM protein and the intracellular tail that connects with talin, which itself binds to the filamentary actin. The integrins therefore mediate the connection between the structural fibres of the ECM and the structural filaments of the cell cytoskeleton. This connection allows an exchange of forces between the extracellular matrix fibres and the strands of the cytoskeleton. The connection is basically a mechanical connection and has consequences on the shape of the cell. Adhesion with integrins also generates important signals for cell life that are directed to the nucleus.

3.2 In vitro cell-matrix interaction

From what is described in the previous paragraphs, the importance of cell-matrix interaction in the regulation of all cellular functions is evident. It is for this reason that biomaterial science is trying to appropriately engineer materials to meet the most common needs of biomedical applications. Until recently, the only two characteristics that a biomaterial had to possess were biocompatibility (the material must not be either cytotoxic or immunogenic) and biodegradability (the material must be easily eliminable once it has fulfilled its function). Today, a biomaterial must have the ability to interface with the biological environment and modulate cell response. The biomaterial becomes, therefore, not only a support for the regeneration of a tissue or a vehicle for the transport of a drug, but also an active part in the regulation of cellular functions. When designing a biomaterial, therefore, it is necessary to take into account the different parameters that can influence the cell-material interaction, and therefore cell response. Cell behaviour is influenced by three characteristics of the ECM: (a) macromolecular components defined by charge, hydrophobicity, amino acid sequence and carbohydrate modifications; (b) Mechanical: the three-dimensional architecture and nanoscale surface topography of cell-binding epitopes; (c) Physical: the elasticity module and resilience of the ECM.[36]

3.3 Effect of micro and nano topography on cells

With regard to surface topography, contact between a cell and a surface can be guided by a surface topography with a specific direction, as grooves, both in the microscale and nanoscale. This phenomenon is called contact guidance effect: cells respond changing their adhesion and

proliferation rates, and/or by alignment, elongation and movement toward the main axis of the grooves.[38] This phenomenon is probably due to a mechanical stress induced by superficial topography on the cells, which causes rupture and the formation of a new cellular fibrous component, influenced cell diffusion and caused alignment.[38] The topography characterized by microgrooves aligns not only the cells, but also their nuclei. A compression of the nucleus causes changes in gene regulation.

In vitro, when a cell is brought into contact with a surface initially it has a roundish shape and the first integrins begin to interact with the substrate. Then the cell begins to explore the surrounding territory through cytoplasmic protrusions. If the surface is suitable for the cell it begins to interact with it and adhere completely to it and first links begin to form. These links are precursors of focal adhesion and they are called close contact. The cell continues to spread to maximize the interaction with the surface and change morphology and finally start the formation of stronger links called focal adhesion.

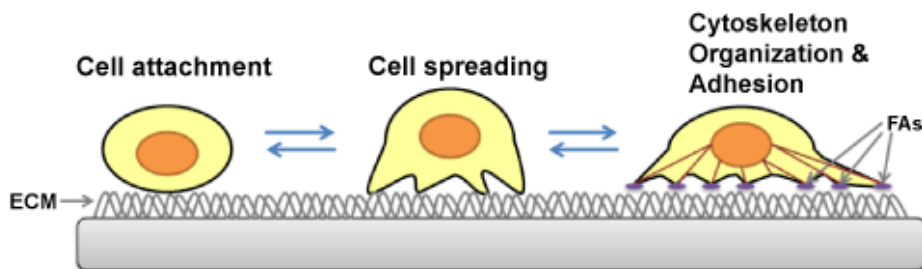


Figure 3.20: Cell-surface interaction and adhesion through the formation of focal adhesions (Fas)

Once the cell has adhered to the surface it uses structures such as filopodia and lamellipodia to explore the environment and move. Filopodia probe the environment around the cell and their ends serve as anchor points for movement. As these structures have sizes in the nanometre range (250–400 nm) it is likely that they will be influenced by nanotopography. It has been shown in the previous paragraphs that integrins are the main responsible for the link between a cell and a surface. As said, integrins are heterodimer proteins constituted of two subunits α and β , and they are in the nanometre scale (8-12 nm). When a cell adheres to a surface, the integrins group together and form complexes known as focal contacts, these are in the micrometre scale. A distinction can also be made between focal complexes measuring $<1 \mu\text{m}$, focal adhesions measuring from 1 to $5 \mu\text{m}$ and super-mature adhesions measuring $>5 \mu\text{m}$.[39] Following contact of

a cell with a topographical surface, the information is transferred to the nucleus by direct or indirect mechanisms, which will cause gene modification and consequently a change in cellular behaviour.

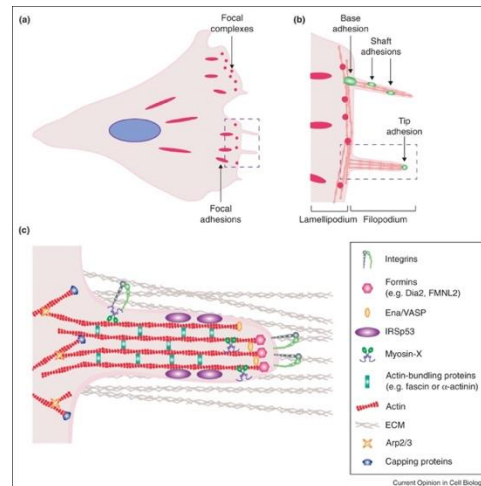


Figure 3.21: (a) Focal complex during cell migration, (b) schematic representation of filopodia, (c) filopodia-ECM adhesion via integrines

Therefore, considering the size of focal complexes (order of microns) and integrins (order of nanometers), the adhesion of cells to a substrate, and later their migration and proliferation, is influenced by the topographies of both scale.

Many authors have studied the interaction between cellular adhesion and surface topography. Below are listed some significant studies to determine the optimal size of grooves.

Walboomers et al. ^[45] carried out a study on a polystyrene substrate, which is used as a reference material for cell cultures. In this study, smooth substrates and substrate with grooves with a depth of 0.5 μm and a width of 1-10 μm were considered. The cells were subsequently cultivated for 4 hours on both substrates and cell response was observed. The cells cultivated on substrates with microgrooves showed rapid alignment along the groove axis. Alignment was faster for grooves 1 μm in size, while it did not occur on smooth surfaces. The results have led to the conclusion that fibroblasts are capable of adhering and proliferating on surfaces with microgrooves.

Su-Yeon Kim et al.[40] have studied the topography of several titanium surfaces, on which human gingival fibroblasts have been cultivated in vitro. They have created microgrooves on dental

implants with a width of 15, 30 and 60 μm and depths of 3, 5 and 10 μm . The results showed that 60 μm large and 10 μm deep grooves were the best in terms of cell proliferation and in gene expression. These measures allow the cells to enter completely into the grooves, colonizing both the edges and the bottom of the grooves. In addition, if the depth increases, the fibroblasts cannot reach the bottom and an optimal contact guidance effect is not permitted.

Yingzhen et al.[41] studied the surfaces of different dental implants by considering fibronectin absorption. This study was carried out on titanium surfaces with grooves with a width of 60, 30 and 15 μm and a depth of 5 and 10 μm . Analysing the results, they found that 60 x 10 size grooves increased wettability of implant and fibronectin absorption.

A. F. Brown et al.[42] have made substrates with grooves of constant depth and amplitude ranging from 1.65 to 8.96 μm . The samples were made with ion-milling technique: a mask with the desired pattern was placed in contact with the quartz substrate and then irradiated by UV rays. Cardiac fibroblasts have been grown on substrates for 24 hours. The results showed that grooves of 8.96 μm were the best in terms of fibroblast adhesion, including the bottom.

Keun Woo Lee et al.[43] have created grooves with constant depths of 3.5 μm and variable amplitude on titanium substrates. Analysis of the results found that for small grooves (2-5 μm) the fibroblasts could not touch the bottom, while for grooves of 30 μm the cells could stick to the bottom of the groove. Through this study it has been demonstrated that the width of the grooves affects the ability of the cells to penetrate into them.

These studies show that microgrooves with a width of 60 μm and a depth of 3 to 10 μm are ideal for caused a correct cellular response.

Fujita et al.[44] have shown that a surface nanopattern can influence the shape and assembly of focal adhesions. In these studies, it has been demonstrated that focal adhesions that formed on the ridges and extended in the direction of the ridge were more stable and resulted in less filopodia retraction than when the focal adhesions were formed perpendicularly to the direction of the ridge. In the first case the focal adhesions are wider, while in the second case they are

fragmented because they only form on the ridges, this involves aligning the cells along the main axis of the nanogrooves (Fig. 3.7).

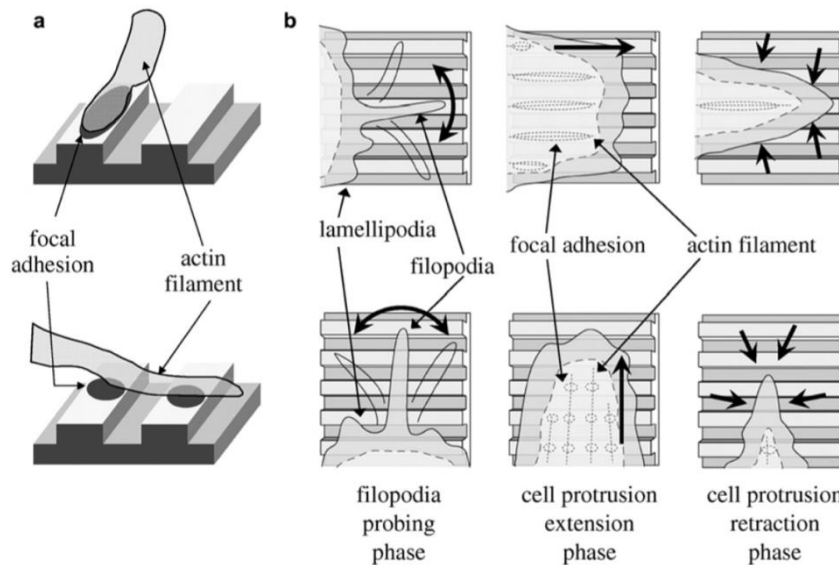


Figure 3.22: Cell alignment on nanogrooves: along the main axis (a), perpendicularly to the direction of the ridge (b)

Loesberg et al.[45] have cultivated cells on polystyrene surfaces. These studies have revealed threshold values that are indispensable to obtain the contact guidance effect of grooves. These threshold values were found to be 35 nm for depth and 100 nm for grooves width. Collagen fibrils are a few tens of nm in size, and this may be the reason for the values obtained. The authors of this study also showed that with increasing groove depth the alignment effect of fibroblasts increased, and the minimum value required for cell alignment was found at 35 nm.

E. Eisenbarth et al.[46] have produced substrates of different materials and with varying roughness. The materials used were cp-titanium grade two, Ti4AlV_a and TiTa30, on which human gingival fibroblasts were cultivated. These authors have shown that the number of aligned fibroblasts increases with increased roughness, regardless of the material. For the smooth surface, the percentage of cells aligned was 11%, while on the substrate with a roughness of $1.36 \cdot 10^3$ nm it was 70%. In addition, after 14 days of cell culture, cell spreading was observed on the cp-titanium grade two and TiTa30 substrates, unlike the Ti4AlV_a substrate where it did not occur.

3.4 Bacteria-matrix interaction

Bacteria are prokaryotic cells, these have a more rigid wall than the eukaryotic cells, consisting of phospholipids. Bacteria can be divided into Gram-positive and Gram-negative: both of them have an external layer of peptidoglycan that made bacterial stiffer than eukaryotic cells. However, this layer is thicker in Gram-positive bacteria, whereas Gram-negative bacteria has a thinner layer covered by an additional polysaccharide outer layer.[39] The size of bacteria varies from under 1 μm to several tens of microns; they are therefore generally smaller than eukaryotic cells. Since the bacteria are more rigid, they retain their shape even after adhesion to a surface. Due to its rigidity, bacteria cannot penetrate into surfaces with a topography smaller than the size of the bacteria themselves.

Bacteria cannot stick individually to the surface, such as eukaryotic cells, but they live on surfaces as communities within a substance called biofilm. When a bacterium comes into contact with a surface, it may establish reversible or irreversible adhesion, depending on the chemical and topographical properties of the material. After adhesion, the bacterium begins to proliferate and synthesize the biofilm, which then becomes mature. The mature biofilm is associated with a specific bacterial metabolism and physiology. Through biochemical signals and membrane organelles, bacteria interact with each other within the biofilm. This allows, for example, the lysis of biofilm matrix molecules necessary for the detachment of biofilm parts and the release of free bacteria into the surrounding environment. The steps in the formation of biofilm may vary according to the biological characteristics of the bacteria, but generally follow the steps listed above.[39]

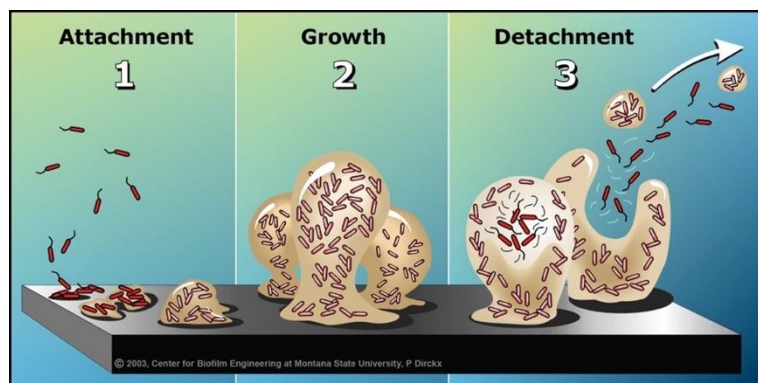


Figure 3.23: Bacterial adhesion step to a surface

However, bacterial adhesion is not yet fully understood compared to cellular adhesion. In addition, unlike eukaryotes cells, bacteria do not require extracellular molecules for adhesion, so they are able to adhere to a surface independently of the presence of ECM. The adhesion of a bacterium to the surface is not based on the link between integrins and ECM proteins as in cells, but is influenced by the physic-chemical properties of the substrate and the bacterial wall.[39]

Although few studies have been carried out, bacterial adhesion mechanism on a surface and the formation of biofilm is fundamental for the creation of surfaces that inhibit bacterial colonisation, and as shown by many authors, when roughness grows, it increases bacterial adhesion on a surface.[38]

Klemen Bohinc et al.[47] have conducted studies on inox steel surfaces. The surfaces used in this study were treated with 3D polishing, brushing, grinding and electropolishing, and roughness has been evaluated by profilometry and atomic force microscopy. The bacterial adhesion rate on the different surfaces was analysed by spectrophotometric measurements. As a result of these measurements, the authors found a higher bacterial adhesion rate on surfaces with higher roughness. In addition, these studies have also demonstrated the influence of surface hydrophobicity on bacterial adhesion.

Al-Ahmad et al.[48] have performed studies on bacterial adhesion with varying surface roughness. They concluded that surfaces with roughness of more than $0.8 \mu\text{m}$ significantly increased bacterial adhesion, while surfaces with roughness less than $0.2 \mu\text{m}$ showed no bacterial adhesion and could be considered smooth for bacteria.

Katrina J. Edwards et al. [49] have shown that the shape of the grooves is the most important influence on the alignment of bacteria, rather than size. In this study, two types of grooves (U-shaped and V-shaped) made on pyrite substrates were examined. The adhesion energy of the bacterium in relation to the characteristic size of the groove has been calculated. The different shape of the grooves can affect bond strength, especially when the characteristic dimensions of the topography are of the same order of size as the bacterium, in particular a higher bond strength has been recorded for the substrate with the U-shaped.

Li-Chong Xu et al.[50] have studied the adhesion of two types of bacteria (Staphylococcus epidermidis and Staphylococcus aureus) on polyurethane films. Polyurethane biomaterial surfaces were textured with ordered arrays of pillars with submicron geometries via a two-stage replication process. Two different diameters were used for nanopillar: 400-430 nm and 500-560 nm, the distance between the pillars was 350-400 nm and 450-500 nm respectively, while the diagonal pillar separation was 680-750 nm and 840-900 nm. The presence of nanopillar has reduced the accessible area for bacteria (more than 70%), this has resulted in a drastic decrease in bacterial adhesion on structured surfaces compared to smooth surfaces. Thanks to this study, the authors demonstrated the existence of alternative methods to chemical and biological modifications to inhibit bacterial adhesion and biofilm formation, using ordered surface texturing patterns

3.5 Optimal grooves for fibroblast [38]

In conclusion, based on literature data, some authors have hypothesized the optimal size of grooves.

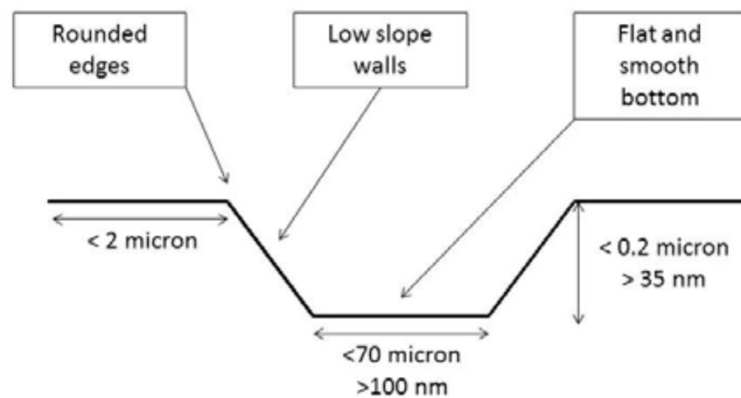


Figura 24

Grooves must have a width of around 20 μm (in particular more than 100 nm and less than 70 μm) so that the cells themselves (fibroblasts) can reach the bottom. If the grooves are tighter, the cell alignment is higher but takes longer time. As regards the depth of grooves, it must be less than 0.2 μm to avoid bacterial adhesion, and greater than 35 nm to be larger than the collagen fibrils. To ensure that cells adhering to different grooves are interconnected, grooves ridges must be smaller than 2 μm . Fibroblasts are also wrinkled cells: a smooth bottom and rounded edges would therefore be better.

These characteristics of the grooves maximize the guide effect on fibroblasts, promoting cell adhesion and reducing bacterial adhesion.

4. Materials and methods

4.1 Sample preparation

This thesis work has been carried out on samples of Ti15Mo, with dimensions of 10 mm x 15 mm and 2 mm of thickness. These were grinded and polished with a *Struers Tegramin-30* machine, in order to remove surface imperfections and obtain mirror polished surfaces.



Figure 4.25: Struers Tegramin-30 machine

Initially the samples were polished using the manual preparation on both sides, to remove the main dirt, using a 320 silicon carbide abrasive paper for a few minutes on each side. The samples were then fixed to a metal disc using adhesive tape and glue in order to polish one of the surfaces. This way made it possible to prepare 6 or 12 samples at the same time (Fig 4.2).

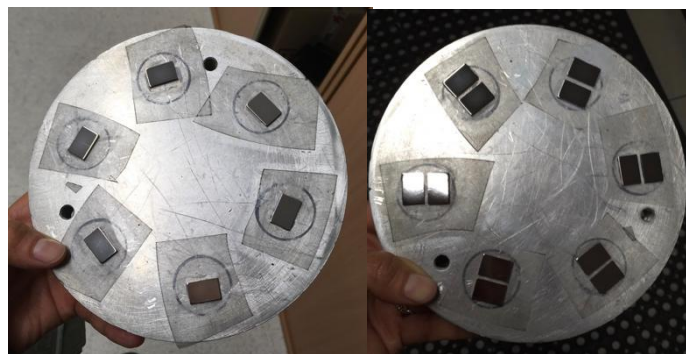


Figure 4.2: Samples fixed to the metal disc

Samples were grinded using silicon carbide abrasive papers with different grit sizes: P320, P800, P1200, P4000, for about 6 minutes per paper. Every 3 minutes the paper was replaced to avoid damaging the samples. After every paper change, samples were washed with water and ethanol and well dried. The process parameters used were: a speed of 150 rpm and a force of about 10 N per sample. During the process water lubrication was performed.

At the end of this operation, samples were polished using a CHEM paper with a solution of 1:5 OPS *Nondry* and distilled water, for about 12 minutes. To remove OPS the samples were subsequently washed with water and ethanol and well dried.

At the end of the polishing operation, the samples were detached from the metallic disc. In order to eliminate contamination, the samples were submitted to ultrasound with acetone for about 5 minutes.

Finally, the specimens were rinsed thoroughly with distilled water and ethanol, and dried with hot air.



Figure 4. 3: Mirror polished samples



Figure 4.4: dirty samples as received vs mirror polished samples

4.2 Electron beam (EBW)

The electron beam welding (EBW) machine type *EBG 45-150 K14* was used to modify the specimen's surface and to produce surface microstructures. The high energy of the electron beam transmitted to the material, causes local evaporation and forms cavities. With the EBW we obtained a microstructure on the surface of 10 μm and 30 μm . This structure is the one that should influence the cell behavior.



Figure 4.5: Electron beam welding machine

The figure file for the EBW machine was build using Matlab. The file consists of x, y coordinates, ordered in two columns. The file for line spacing of 10 μm consists of 122848 points and for 30 μm 41184 points. The X and Y amplitude (figure size) was set as 7 mm, respectively. The most important machine parameters, voltage and current, where set constant, and the deflection velocity was changed respectively for line spacing (for 10 μm 3333 mm/s and 30 μm 853 mm/s).

Machine parameter (constant):

- 150kV voltage
- 0.8mA current

The samples were positioned as shown in the figure below and were washed with alcohol before placed inside the machine.

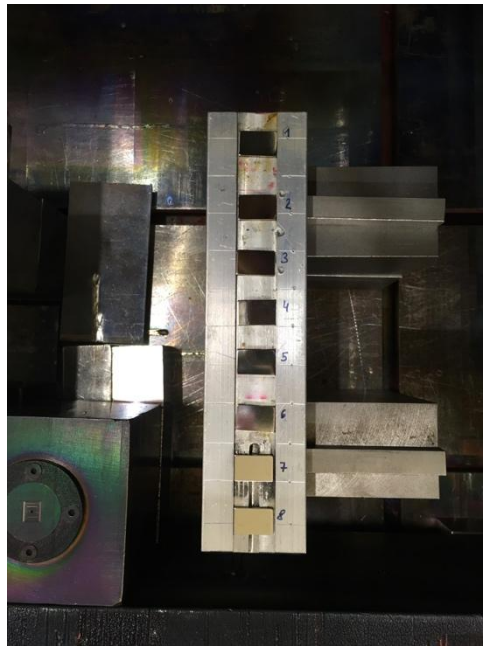


Figure 4.6: Samples placed in the machine

At the end of the process it is possible to observe the microstructure on the surface of the samples (Fig. 4.7).



Figure 4.7: Microstructure sample after EBW

4.3 Cutting of samples

The micro structured samples have been cut by the machine *Struers Accutom-2* in order to obtain from each sample four pieces of approximately 3.5mm x 10mm in size (Fig. 4.10), for subsequent heat treatment. The discs used for cutting the samples were type *10S15* or *50A15* for non ferrous materials.



Figure 4.8: *Struers Accutom-2* machine

After cutting, the samples were put in ethanol inside the ultrasonic machine for about 3 minutes per sample, to remove any dirt.

At the end of the cutting operation, the part used to fix the sample to the machine was divided from the others and named as “Rest cut”.

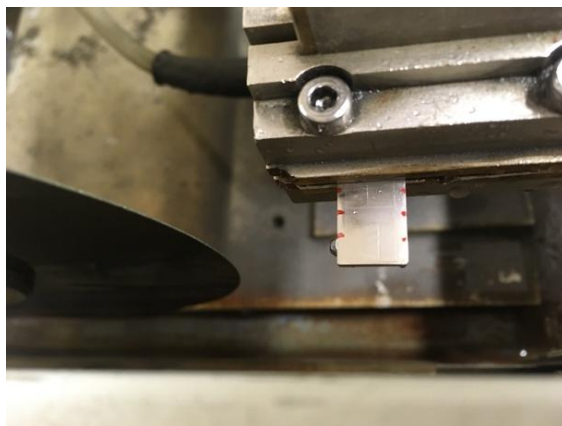


Figure 4.8: Sample fixed to the machine



Figure 4.10: Cut samples

4.4 Dilatometry

After EBW, the samples were subjected to heat treatment (HT) to investigate phase transformation and changes in microstructure. The different parameters used are shown in the table 4.1.

	<i>T</i>	<i>Heating rate</i>	<i>t</i>	<i>Sample</i>		<i>Atmosphere</i>
1	500° C	5 K/min	4h	30 μm	Rest cut	Vacuum
2	500° C	5 K/min	8h	10 μm	Rest cut	Vacuum
3	550° C	300 K/min	4h	10 μm		Vacuum
4	500° C	300 K/min	4h	10 μm		Vacuum
5	600° C	300 K/min	4h	10 μm		Vacuum
6	600° C	5 K/min	4h	10 μm		Vacuum
7	550° C	5 K/min	8h	10 μm		Vacuum

Table 4.1 Parameters of heat treatment

HT influences the internal morphology of the material: it is possible to see α phase in the β titanium alloy after this treatment. Initially the material at room temperature was all in beta

phase, after HT there will be a matrix of β phase, different morphologies of α phase and α grain boundary. At this point the surface of the material should have the microstructure obtained by EBW and α grains.

After ageing, the microstructures may be expressed as a function of different parameters, as shown below:

$$F(\dot{T}, T, t, S_0)$$

\dot{T} = heating rate

T = temperature

t = time

S_0 = initial microstructure

To create a nanostructure on the surface of the specimens, samples were subject to chemical treatment. Different etching times and different solutions were used for this purpose. At first, etching has been applied to the structured surface of the samples with a solution of *85 ml distilled H₂O, 5 ml hydrofluoric acid, 10 ml nitric acid*. Different etching time were applied, as shown in the table 4.2.

<i>Sample</i>	<i>Etching time</i>
<i>Sample 1</i>	3 s
<i>Sample 3</i>	3 s
<i>Sample 2</i>	5 s
<i>Sample 4</i>	5 s
<i>Sample 7</i>	10 s

Table 4.2: Etching time

4.5 Furnace

As regarding the heat treatment, furnace was used instead the dilatometry for four samples. The different parameters are shown in the table 4.3.



Figure 4.11: Furnace

	<i>T</i>	<i>Heating rate</i>	<i>Time</i>	<i>Sample</i>
1	600° C	50 K/min	2h	10 μm
2	600° C	50 K/min	4h	10 μm
3	550° C	300 K/min	4h	10 μm
4	550° C	5 K/min	4h	10 μm

Table 4.3: parameters furnace

After the furnace, the samples were mounted in the polyfast powder in order to analyze the cross section by LOM and SEM and the grinding and polishing steps were performed as described below.

4.5 Metallography

To analyze simultaneously the base material and the surface of previous samples, they have been mounted in the polyfast powder (Fig. 4.12), so that the cross section can be analyzed. The samples were then analyzed by SEM characterization following grinding and polishing steps.



Figure 4.12: Samples in the polifast powder

The samples have been fixed by sample holders for semiautomatic polishing machine, as shown in the following picture.



Figure 4.13: Sample holder for semiautomatic polishing

As regarding the grinding and the polishing the *Struers Tegamin-30* machine has been used. Silicon carbide abrasive papers with various grit size were used with force of about 10 N per sample and a speed of 150 rpm.

The different process parameters of the grinding and the polishing are shown in the table 4.4 and table 4.5.

Grinding step:

P. 300	3 min	H ₂ O
P. 500	5 min	H ₂ O
P. 1200	10 min	H ₂ O
P. 4000	10 min	H ₂ O

Table 4.4

Polishing step:

P. 1 µm	10-15 min	Nap Dia Duo-2
P. CHEM	20 min	OPS 1:5
P CHEM	3 min	H ₂ O

Table 4.5

At the end of the process, samples were cleaned with water and alcohol and well dried.

At this point, the samples were etched for a time of 3 seconds each, in a solution of *85 ml distilled H₂O, 10 ml hydrofluoric acid, 5 ml nitric acid*. LOM analysis was then carried out.

4.6 Sample washing and sterilization

To carry out tests with cells and bacteria and surface characterizations, 36 samples measuring 10 mm x 7.5 mm were brought to Politecnico of Torino (Fig. 4.14). The samples were made at Technology University of Graz with the following characteristics:

- 12 samples mirror polished (MP)
- 12 samples with a microstructure of 10 µm (EB 10)
- 12 samples with a microstructure of 30 µm (EB 30)

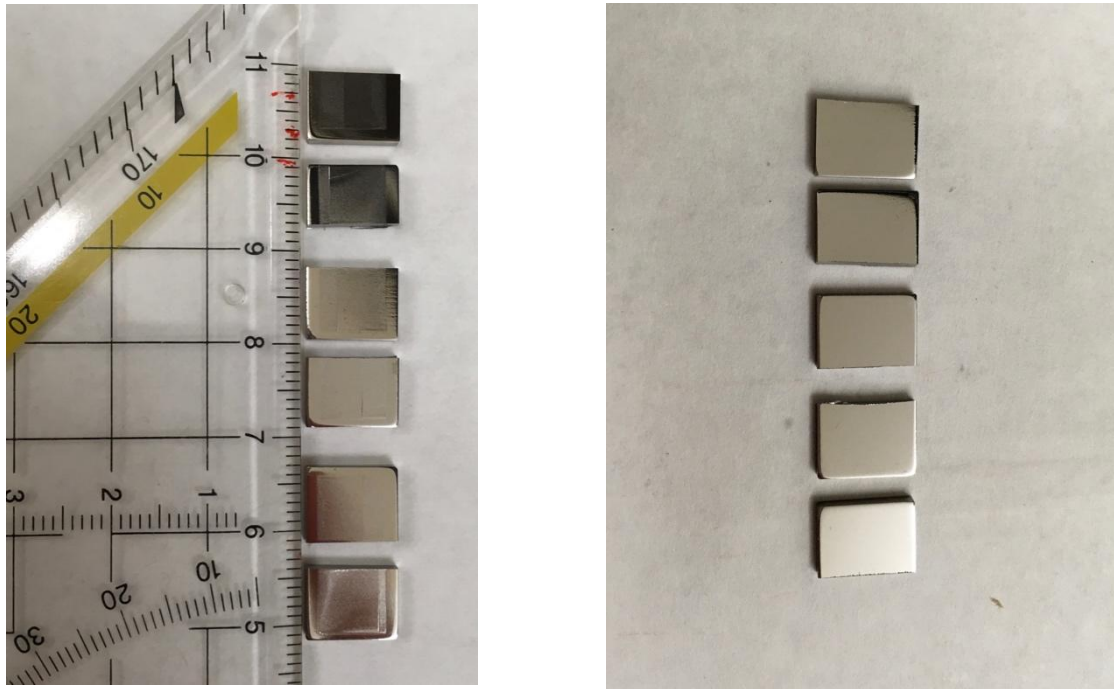


Figure 4.14: EB 10 samples and MP samples

In order to eliminate contamination introduced on the surface of the samples as a result of previous operations and transport, the samples were washed in ultrasound. In particular, three washes were conducted, all at room temperature.

For the first wash the samples were immersed in acetone, taking care to position the structured part upwards and the unstructured part in contact with the beaker bottom. This operation was carried out under the fume hood and then the containers, covered with aluminum foil, were inserted into the sonication for a period of 5 minutes. At the end of 5 minutes, the samples were transferred under the hood and immersed in a baker with distilled water. Bakers were then placed in the sonication for 10 minutes. This last wash was repeated a second time with new distilled water.

All these operations were carried out using 3 different beakers for the 3 types of samples.

The samples were then dried and placed in Petri dishes and sterilized in the furnace for 2 hours at 180 °C. At the end of the operation the samples were packed in sealed bags.

Finally, one sample by type was subjected to heat treatment in the oven at a temperature of about 540 degrees for 4 hours, in vacuum condition.

The washing and sintering steps of the samples are summarized in the following table.

	<i>Time</i>	<i>Temperature</i>
Acetone	5 min	Room T
Distilled H ₂ O	10 min	Room T
Distilled H ₂ O	10 min	Room T
Furnace	4 h	180 °C

Table 4.6: Washing and sintering steps

4.7 Cell and bacteria test

Cell and bacterial tests were carried out at Novara's laboratories to evaluate adhesion on smooth and grooves (10 μm and 30 μm) samples. In particular, three samples per type (MP, EB10, EB30) have been used for both cell tests and bacterial tests, using a glass sample as control.

As regards cells, primary human gingival fibroblasts (HGF) have been used, as the material is intended for dental implants. Each sample was placed in a well and covered with a 100 μL suspension containing 20000 cells on DMEM medium with 10% FBS and 1% antibiotic (Fig. 4.15). The cells were then cultivated for 48 hours.

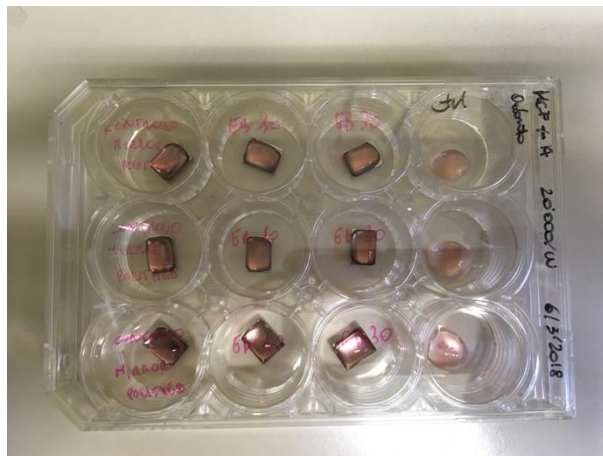


Figure 4.15: Samples within wells for cell test

Staphylococcus aureus has been used for bacterial tests, since these are the most difficult to remove among bacteria that cause infections in dental implants. In this case each sample was placed in a well and immersed in a suspension of LB medium and bacteria (Fig. 4.16).

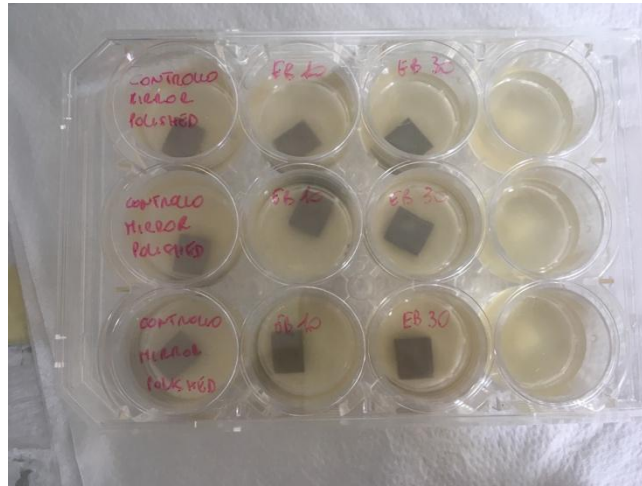


Figure 4.16: Samples within wells for bacteria test

4.8 Characterisation methods

4.8.1 Scanning Electron Microscope (SEM)

The scanning electron microscope was used to observe the samples subjected to electron beam and to analyse changes in the microstructure of the material following heat treatment.

The Scanning Electron Microscope (Fig. 4.17) exploits a beam of focused primary electrons that hit the sample, unlike the optical microscope that uses light as a radiation source. The beam is generated by an electronic source, concentrated by a series of electromagnetic lenses and deflected by an objective lens. The latter, in addition to refocusing the beam, imposes a controlled deflection on the beam to allow the scanning of sample areas. When the beam impacts on the sample to be observed, this responds by emitting a series of particles including secondary electrons that are captured by a special detector and converted into electrical pulses. The electrical signal generated by secondary electron processing is sent to a monitor where a similar scan is performed. The result is a black and white image that has characteristics similar to those of a normal photographic image and therefore immediately intelligible and intuitive to understand. The images are equipped with a high depth of field that allows to observe the surface of the sample in every detail, being able to identify even the smallest metallurgical defects or detect unexpected precipitated phases. The resolution power of a tungsten cathode electron microscope is around 5 nm, while the acceleration voltages of electrons vary from 0.5 to 30 kV. Preparation by

polishing the surface of the sample to be observed is of fundamental importance. The arrangement of the samples in the machine takes a long time because the sample must be taken under vacuum at a pressure of about 10^{-5} Torr. In addition, the sample must be conductive or properly metallised, otherwise the piece is not able to emit secondary electrons. Due to the much shorter electron wavelengths than photons, the resolution power of a scanning electron microscope is significantly higher than an optical microscope.[51]

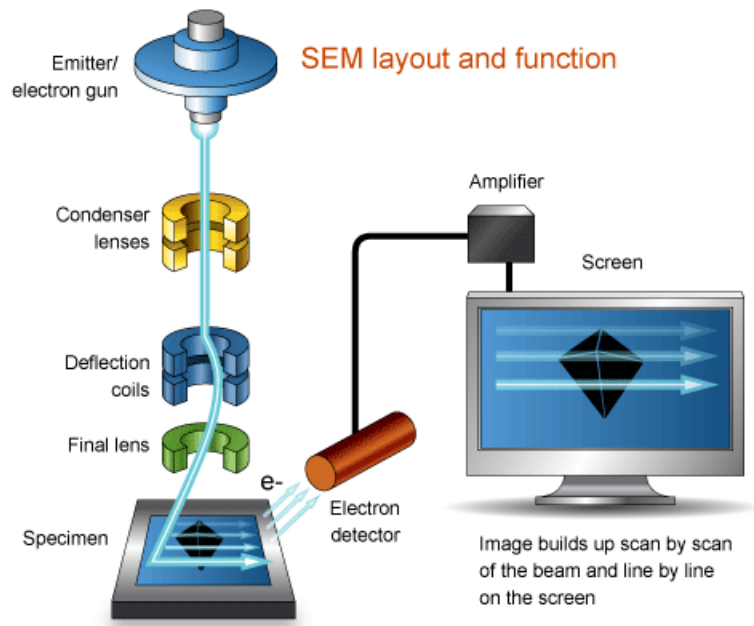


Figure 4.17: Scanning Electron Microscope

4.8.2 Surface roughness

Roughness measurements were taken to describe the topography of microstructured samples. This parameter is indeed very important in determining the behaviour of cells and bacteria when they come into contact with the surface. Average roughness R_a is the most common and universally recognized parameter for roughness evaluation. R_a , expressed in microns, is defined as the arithmetic mean of the absolute distances of the roughness profile to the mean line. [52]

$$R_a = \frac{1}{L} \int_0^L |y(x)| dx$$

However, the Ra value is not sufficient to completely define the morphological characteristics of the surface, as profiles with different trends from the same arithmetic mean deviation will have the same value as Ra; for this reason, other parameters have been introduced, such as Rq (Rms: root mean square). Rq is the square mean of the deviation of the profile points from the midline. This parameter, being a quadratic average, is more sensitive to sharp deviation of the profile from a regular pattern and is generally higher than the Ra value.[52]

$$Rq = \frac{1}{L} \int_0^L |y^2(x)| dx$$

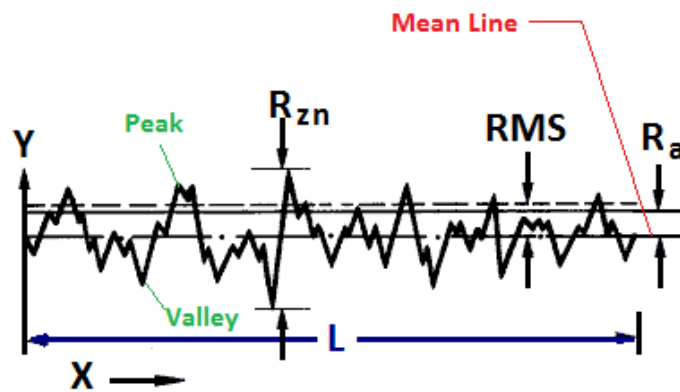


Figure 4.18: Roughness parameters

Surface roughness measurements were carried out at CNR in Turin using a *Taylor-Hobson* mechanical profilometer. An optical profilometer model *Talysurf CCI 3000* was used to obtain two-dimensional profiles and three-dimensional images. The measurements were carried out on the following sample types:

- Mirror polished sample (MP)
- Microstructured samples 10 μm (EB 10)
- Microstructured samples 30 μm (EB 30)
- Heat-treated mirror polished sample (MP HT)
- Heat-treated microstructured samples 10 μm (EB 10 HT)
- Heat-treated microstructured samples 30 μm (EB 30 HT)

The parameters of heat treatments were 540 $^{\circ}\text{C}$ for 4 hours in the furnace.

4.8.3 AFM

The Atomic Force Microscopy (AFM) is a scanning probe microscopy (SPM). It consists of a cantilever at the end of which is mounted a sharp tip, typically composed of silicon or silicon nitride, which has a radius of curvature in the order of nanometres. The instrument scans the sample using this tip. During scanning, weak forces of interaction between tip and sample are established, which result in a deflection of the cantilever and consequent detection of the surface topography. Cantilever deflections until 0.01 nm can be detected by an optical system consisting of a laser, reflected from the top of the cantilever itself, and photodetector (Fig 4.19). This system is especially important in the analysis of biological materials, because it allows to apply a minimum force on the sample limiting the damage. [53]

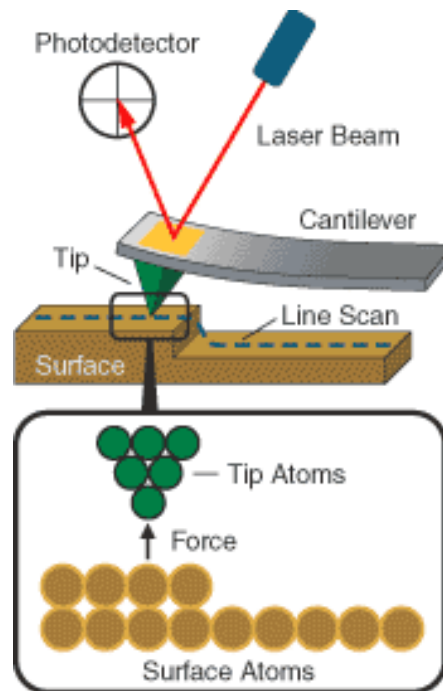


Figure 4.19: AFM components

AFM was therefore used to scan the microstructured samples (EB10 and EB30) and reconstruct their surface topography. In particular, the instrument used was *Bruker Innova*[®] Atomic Force Microscopy (Fig. 4.20). The tip used was model RESPA-20, positioned vertically on the grooves. 2D and 3D images of the sample surface were processed using *Gwyddion 2.48* software. In addition, a colour scale provides information about depth: dark colours indicate deeper areas while light colours indicate shallower areas.



Figure 4.20: Bruker Innova® Atomic Force Microscopy

4.8.4 Contact angle

Wettability indicates the ability of a liquid to maintain contact with a solid surface, linked to intermolecular interactions that are present when the liquid and surface come into contact. The degree of wettability is determined by the balance between the adhesion forces and the cohesion forces of the liquid itself. Adhesion forces are attractive forces between different molecular types, while cohesion forces are attractive forces between molecules of the same type. The contact angle allows to evaluate the wettability of a surface: the lower the contact angle, the higher the degree of wettability. Contact angle is the angle formed by the encounter of a liquid-vapour interface with a liquid-solid interface: is the angle between the tangent to the surface of the drop and the surface on which it is placed. [54]

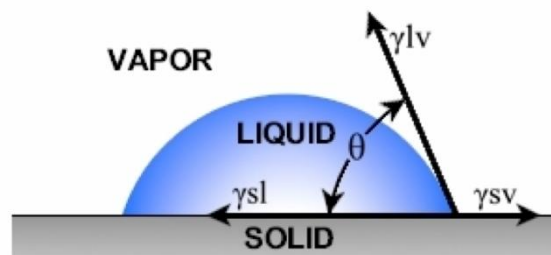


Figure 4.21: contact angle

For an ideal surface, smooth and homogeneous, the contact angle is based on the thermodynamic equilibrium of three phases (solid, liquid, vapour) and is defined by Young equation: [54]

$$\gamma_{SV} - \gamma_{SL} - \gamma_{LV} \cos \theta = 0$$

The parameters present in the equilibrium condition are: [55]

- γ_{SV} : energy at the interface of the solid and vapour phase;
- γ_{LV} : energy at the interface of the liquid and vapour phases;
- γ_{SL} : energy at the interface of the solid and liquid phases.

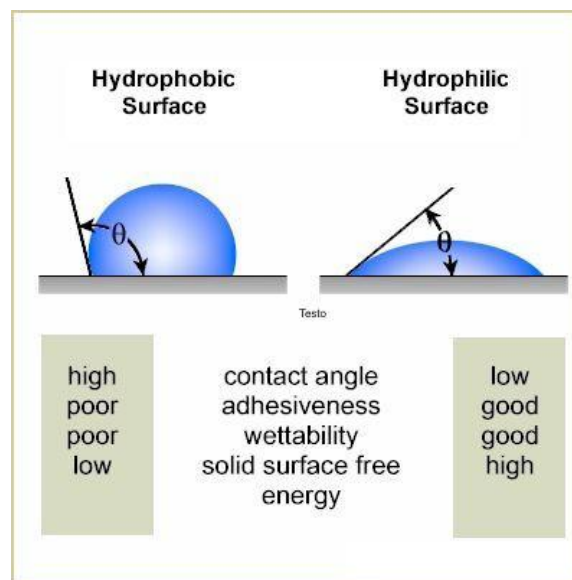


Figure 4.22: difference between hydrophobic and hydrophilic surface

In the particular case of water, a surface can be defined as follows:

- Hydrophilic if $0 < \theta < 90^\circ$
- Hydrophobic if $90 < \theta < 150^\circ$
- Superhydrophobic if $\theta > 150^\circ$

Wettability measurements were carried out on mirror polished samples and on structured samples (10 μm and 30 μm). The equipment used consists of a support plate for the sample, on which a liquid drop is placed through a micrometric pipette, a light source and a telescope connected to the software. The two-dimensional image and contact angle measurement are reconstructed by software. The liquid used for this test was distilled water. A constant drop of volume was created (5 μL), placed on the sample surface and a static contact angle was measured. On each sample type, different measurements were carried out by placing several drops on the surface of the samples.

4.8.5 XRD [55]

X-ray diffraction (XRD) is a non-destructive technique used to determine crystalline phases contained in minerals. The technique also allows, through calculation software, the structural-crystallographic study (shape, size and characteristics of the elementary cell), as well as the microstructural analysis of the crystalline phases present in the material under examination. The X-rays used are electromagnetic radiations characterized by a wavelength comparable to the interatomic distance: penetrating deep into the matter due to their low absorption coefficient, they generate diffraction phenomena that allow to obtain information on atomic positions and their nature. When an X radiation hits an atom, the internal electrons enter into oscillation: each atom can be considered a source of a spherical wave with an intensity proportional to the number of its electrons. Diffuse waves give rise to constructive or destructive interference in space and are at the origin of diffraction phenomena. The working principle of an X-ray diffractometer is based on Bragg reflection or diffraction: the phenomenon of diffraction from a crystal can be described as a selective reflection of monochromatic radiation by atomic planes. A collimated beam of monochromatic X-rays is reflected from adjacent and equivalent crystalline planes, generating an interfering structure of intensity peaks, called diffraction patterns, in the surrounding space. Each crystalline phase is associated with a certain number of diffraction peaks (Bragg peaks), which allows their recognition by comparison with standard reference cards.

The instrument works as follows: a beam of parallel and monochromatic X-rays (with defined λ) affects the sample, the radiations diffracted by the sample are collected by a detector that transforms them into electrical pulses, which are then amplified and sent to a computer that allows processing.

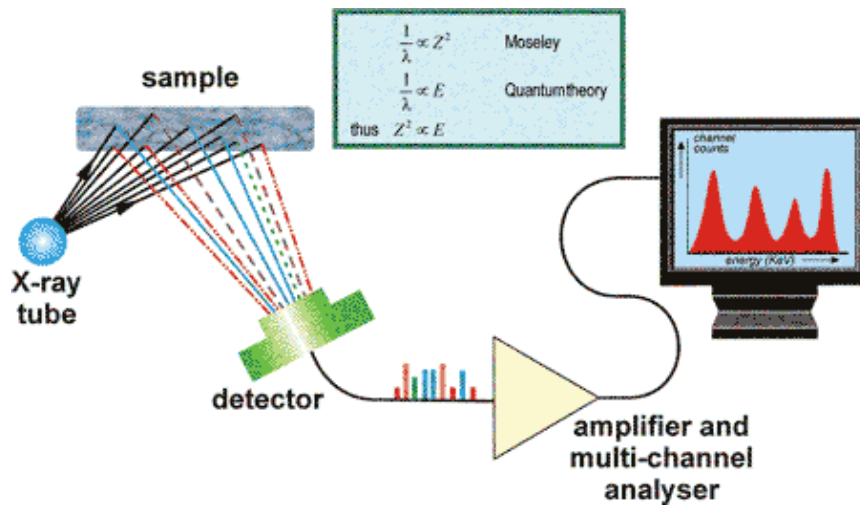


Figure 4.23: X-ray analysis

When an electromagnetic wave is engraved on a crystal, interference phenomena are observed, caused by the reflection of waves from different but parallel crystalline planes. This phenomenon is summarized in Bragg's law:

$$n\lambda = 2d\sin(\theta)$$

- θ is the angle which the outgoing beam forms with the crystalline plane;
- λ is the wavelength of the radiation;
- d is the distance between two adjacent planes;
- n indicates the order of diffraction.

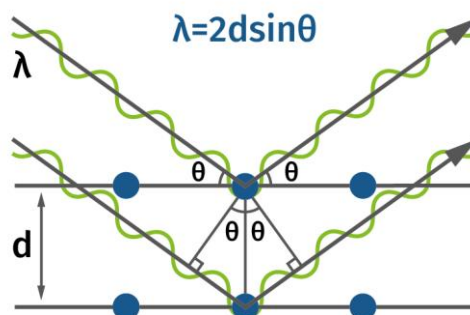


Figure 4.24: 2θ X-ray wave interface

This law may therefore be used to know distances interplanar in the material under examination, varying the wavelength of the incident ray or the angle of incidence θ . If the Bragg condition is fulfilled (the difference in optical path between the various reflected waves is an integer multiple of the λ wavelength), the detector will collect, in the direction of the angle, a peak of intensity of the radiation reflected by the sample.

Diffraction spectrum can provide different information:

1. from the angular position of the peaks, the interplanar distances and therefore the reticular parameters of the material are obtained (qualitative analysis); moreover, it is possible to identify the phases present through the PDF archive (Powder Diffraction File, containing crystallographic information for more than 300000 inorganic and organic phases);
2. from the intensity of the peaks it is possible to carry out a structural analysis, namely the position of the atoms in the elementary cell (quantitative analysis);
3. from the peak width or mid-height amplitude (FMHW) information is obtained on the size of the crystals and on their possible deformation. An XRD measurement is based on the measurement of distances between reticular planes using a radiation source with a wavelength of a few tens of nanometres (nm).

The x-rays were performed on the following samples:

- Mirror polished sample (MP)
- Microstructured samples 10 μm (EB 10)
- Microstructured samples 30 μm (EB 30)

5. Results and discussion

5.1 SEM analysis after Electron Beam

The microstructure of the samples created by electron beam was observed by SEM analysis. From the SEM images it can be seen that the microstructure of 30 μm is clearly visible (Fig. 5.1), beta grains and grain boundaries can also be observed very well (Fig 5.1 b). Instead, for samples with a microstructure of 10 μm (Fig. 5.2) the grooves are much less visible. The image with magnification 250x (Fig. 5.2 a) represents the boundary between the smooth zone and the microstructure zone; in the microstructure area at the top of the image the grooves are more evident, while in the area below they are almost invisible. Furthermore, in the structured area the grains are smaller than in the unstructured area; this is due to the fact that the area subject to electron beam heats and solidifies quite quickly, while in the other area the material heats up causing the growth of grains.

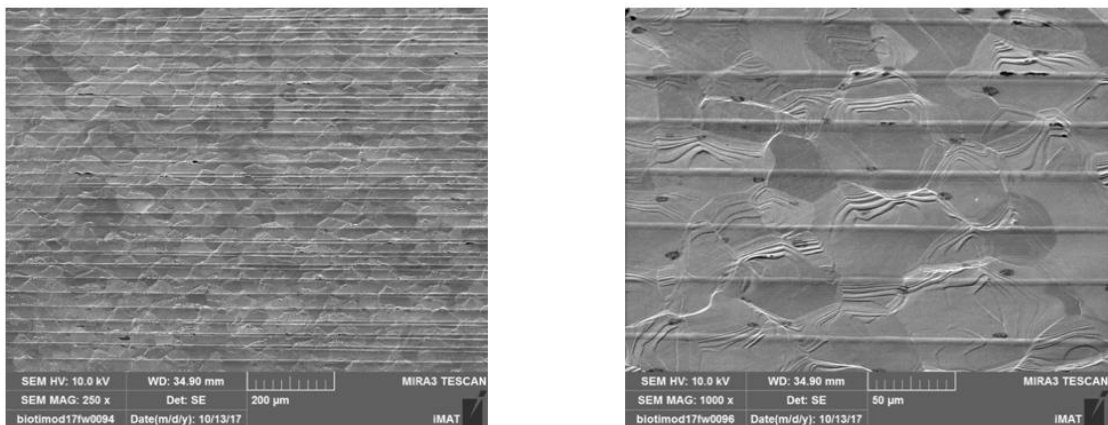


Figure 5.1: SEM images sample 30 μm

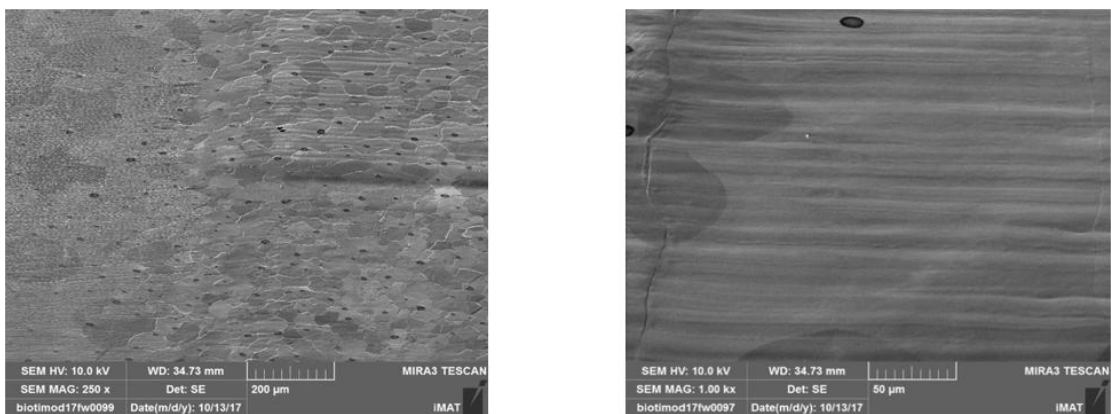


Figure 5.2: SEM images sample 10 μm

5.2 SEM analysis after heat treatment

Changes in the microstructure of heat-treated Ti15Mo samples were analysed by SEM. The analysis was conducted on the cross section of the samples to evaluate any differences in the structured area and base material. From the images we can see how thermal treatments have caused the precipitation of alpha in the beta matrix, obtaining a biphasic alloy. In general, the alpha obtained are very small, reaching nanometre sizes and are concentrated particularly in the grain boundaries.

5.2.1 SEM images after dilatometry

Images of the samples heated to 500°C show a very fine structure of alphas in the base materials. Alphas are present both as black dots and lamellar structure and are clearly visible in the grain boundary (Fig. 5.3 b). A very fine microstructure can also be found from the surface analysis (Fig 5.4b).

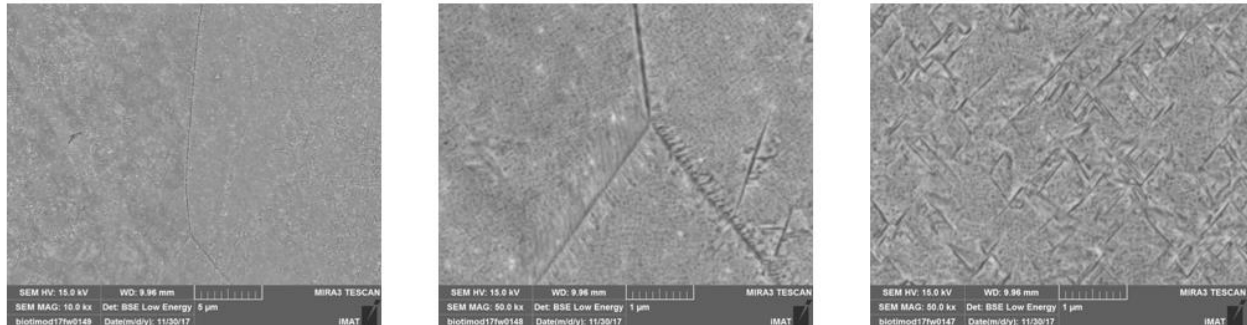


Figure 5.3: SEM images of samples heated to 500°C with 5K/min for 8 hours in base materials

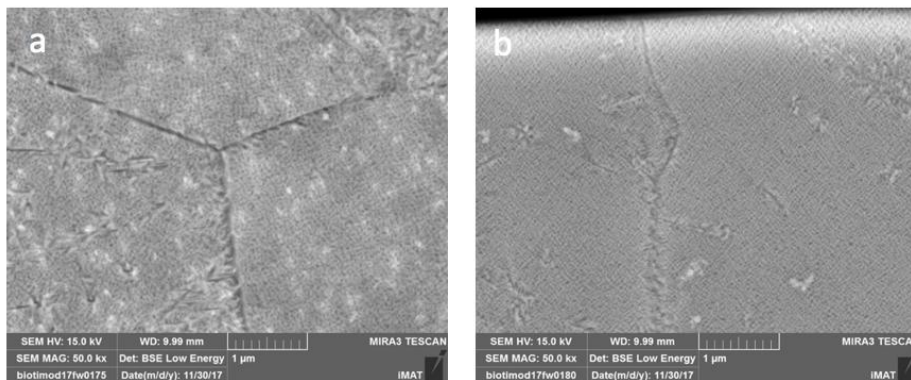


Figure 5.4: SEM images of samples heated to 500°C with 5K/min for 4 hours in base materials (a) and in the surface zone (b)

The microstructure looks similar everywhere in the base material on the sample heated up to 500°C and exposed to heat treatment of 300 K/min (Fig 5.5). Also in this case alphas are very small, but from surface analysis it is possible to observe a certain inhomogeneity, which may be attributed to the processes to which the material has been subjected, in particular to the melting.

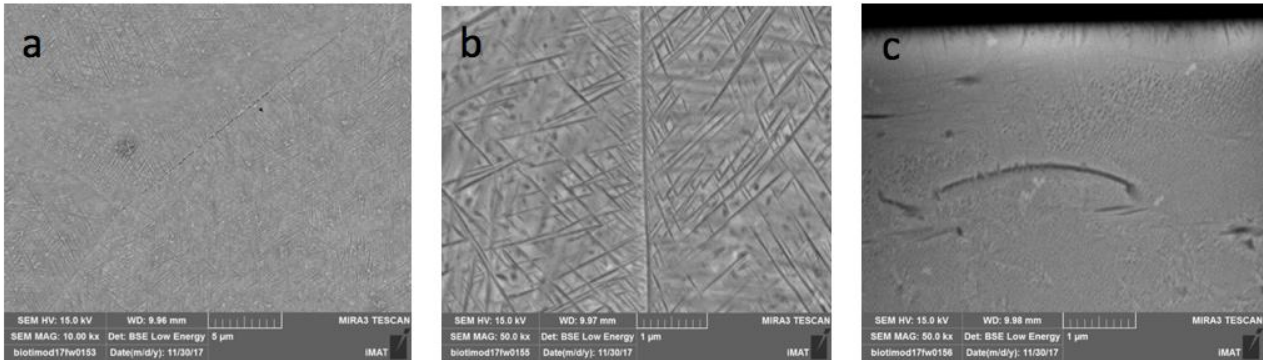


Figure 5.5: SEM images of sample heated to 500°C with 300K/min for 4 hours in base materials (a), (b) and in the surface zone (c).

For samples heated to 550°C, morphology changes significantly compared to earlier samples. From the image of the base material (Fig. 5.6 a, Fig. 5.7 a) it can be seen how full of alphas it is and from the surface analysis (Fig. 5.6 b, Fig. 5.7 c) how small these are: in the order of nanometer (Fig. 5.7 b).

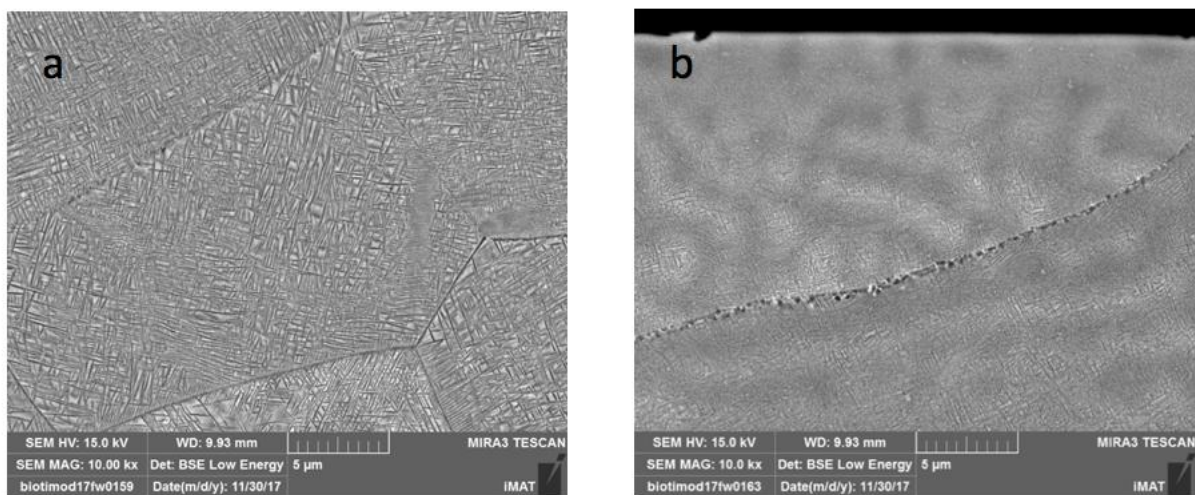


Figure 5.6: SEM images of samples heated to 550°C with 5K/min for 4 hours in base materials (a), and in the surface zone (d).

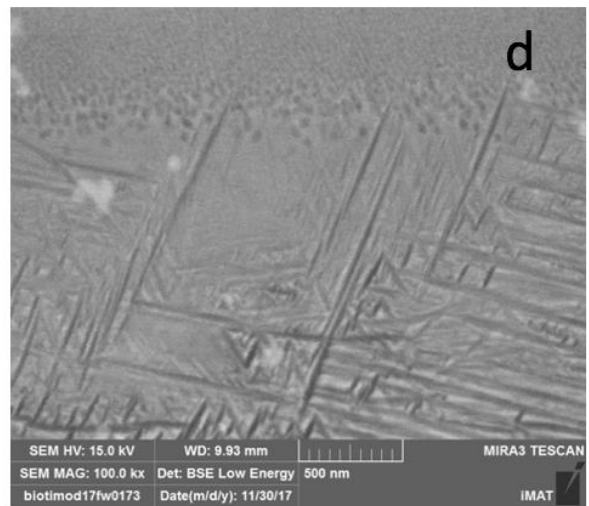
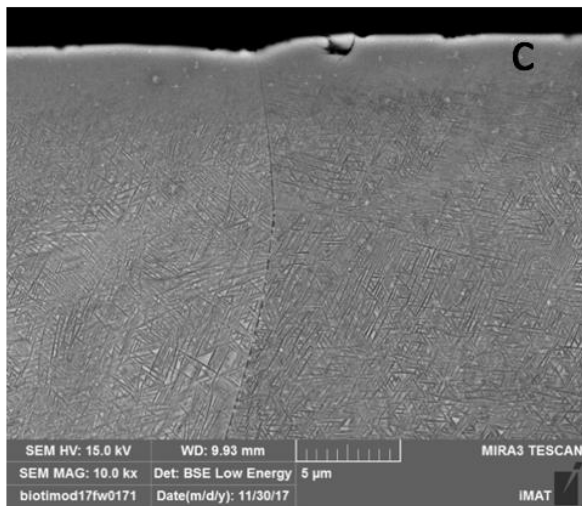
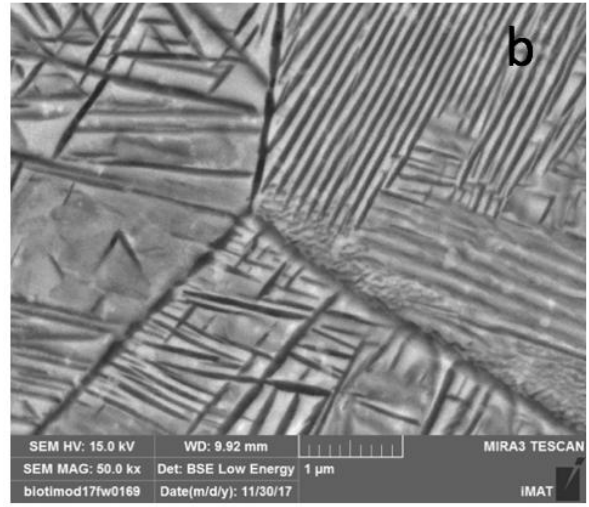
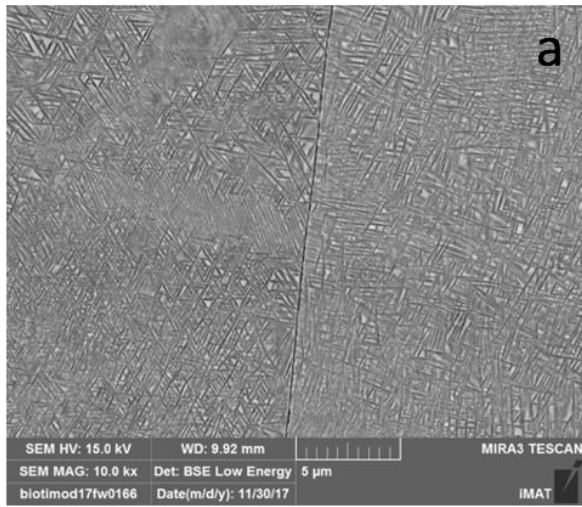


Figure 5.7: SEM images of samples heated to 550°C with 300K/min for 4 hours in base materials (a, b), and in the surface zone (c, d)

5.2.2 SEM images after furnace

By SEM characterization it is possible to see very well the alphas, especially in the grain boundary. For the sample heated up to 600°C the distribution of alphas is homogenous in the base material. Moreover, the alphas are very small with a long laminar shape. It has been measured a maximum length of about 1.97 μm and a minimum of 0.47 μm and a average distance of 0.17 μm between alphas. From the following images it is possible to see that the material is full of alphas. The structured area is very small compared to the base material (Fig. 5.8 c) and a change of the material is observable. Furthermore, it is possible to observe very fine alphas and a more homogeneous distribution of them.

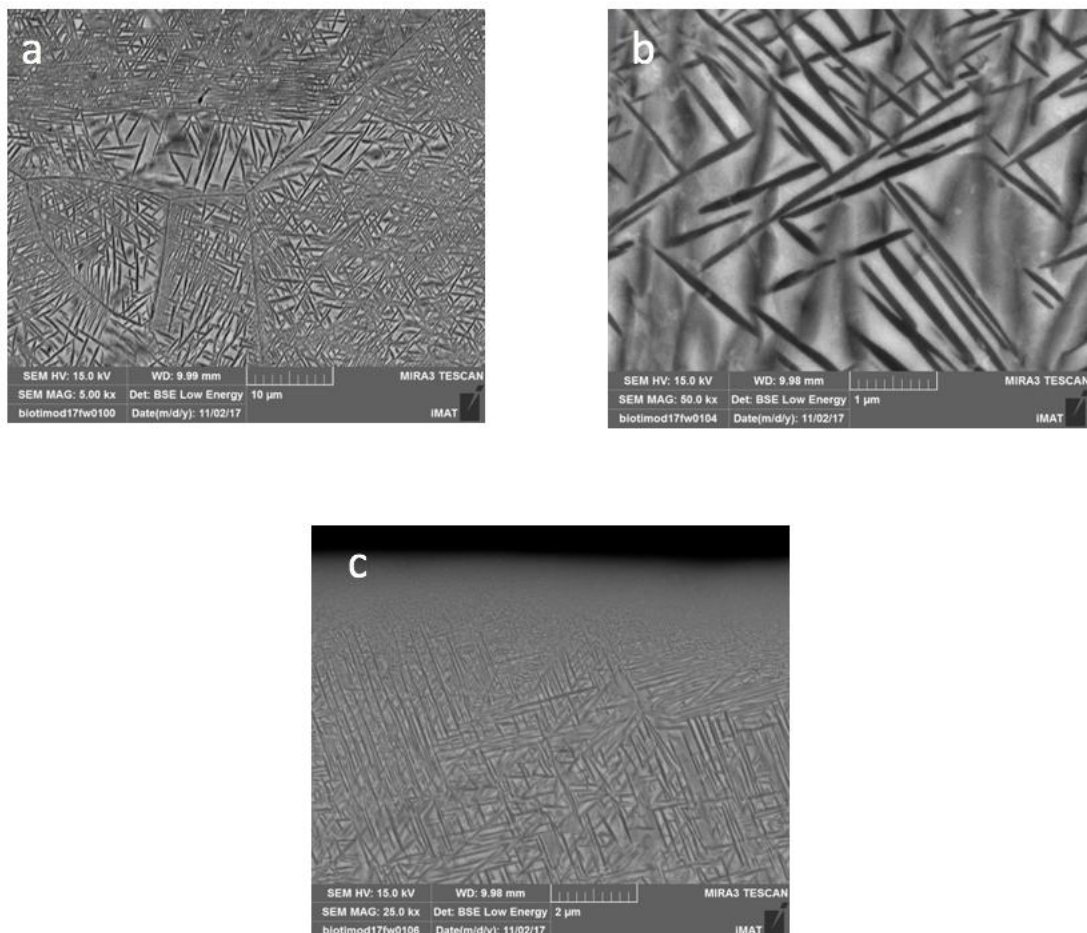


Figure 5.8: SEM images of samples heated to 600°C with 300K/min for 4 hours in base materials (a), (b) and in the surface zone (c)

For the sample heated up to 550°C with 300K/min (Fig. 5.9) it can be observed finer alphas that in the previous sample and also in this case the distribution is homogenous. From the images it can be seen how full of alphas the material is. In this case it has been measured a maximum length of alphas of about 1.45 μm and a minimum of 0.29 μm and a average distance of 0.07 μm between alphas.

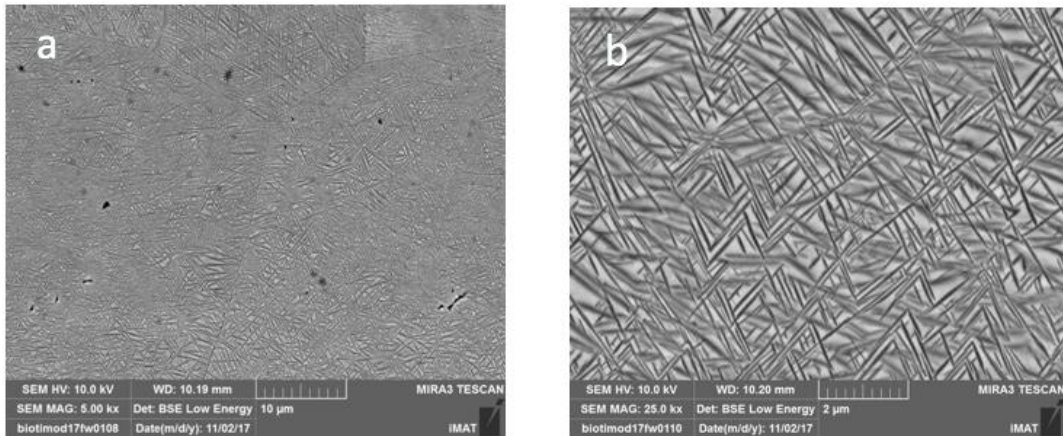


Figure 5.9: SEM images of samples heated to 550°C with 300K/min for 4 hours in base materials

As regarding the sample heated up to 550°C with 5 K/min (Fig. 5.10) the distribution of alphas is more homogenous compared to the other samples. Alphas are shorter with a distance about 0.06 μm between each other.

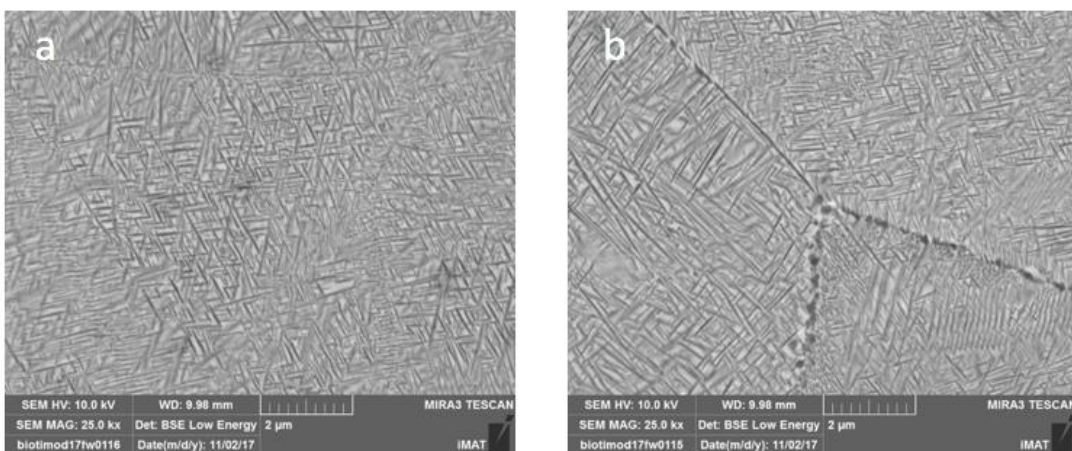


Figure 5.10: SEM images of samples heated to 550°C with 5K/min for 4 hours in base materials

5.3 Etching

As explained in the previous chapter, some samples have been subjected to etching. Images made by light optical microscope (LOM) are shown below.

The samples in figure 5.11 and 5.12 were etched for a time of 3 seconds each, in a solution of 85 ml distilled H₂O, 10 ml hydrofluoric acid, 5 ml nitric acid. It is possible to see the alphas at the grain boundary in the base material and to observe a different morphology of the material in the structured surface compared to the base material (Fig. 5.11 b). In addition, the alphas that can be observed are very fine (Fig 5.12 b).

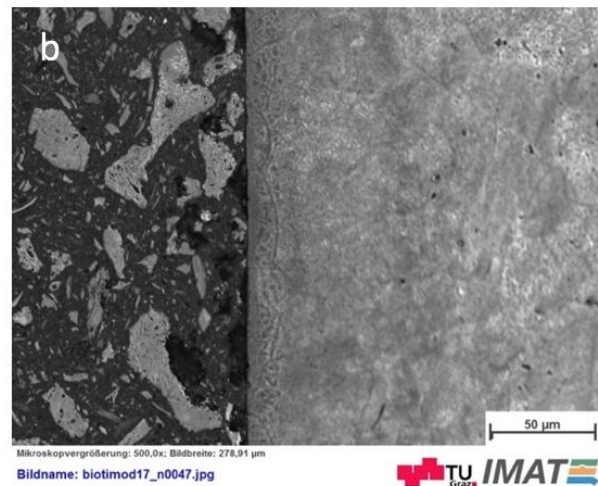
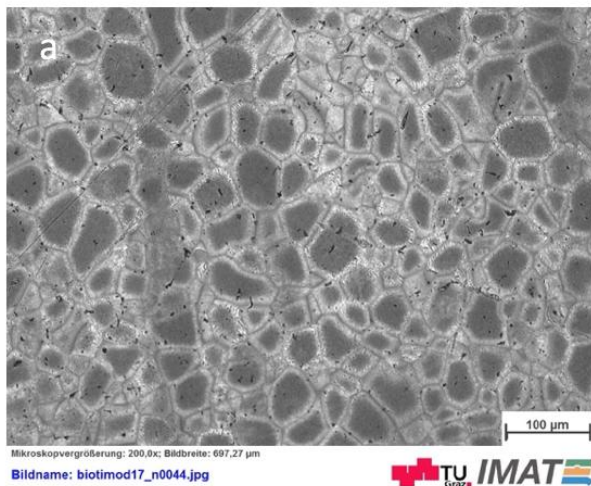


Figure 5.11: LOM images of samples heated to 550°C with 5K/min for 4 hours, base material(a), surface (b)

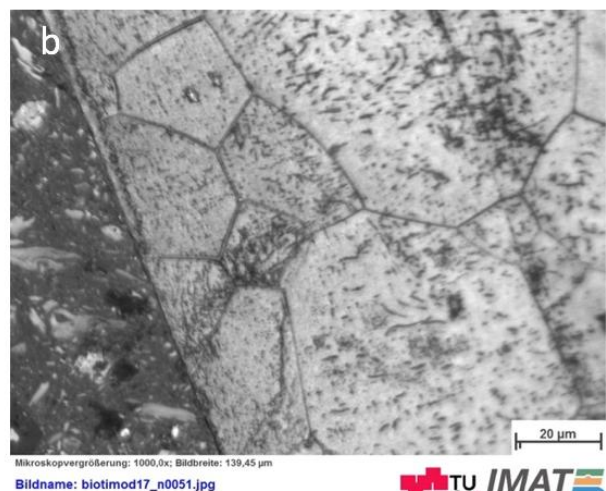
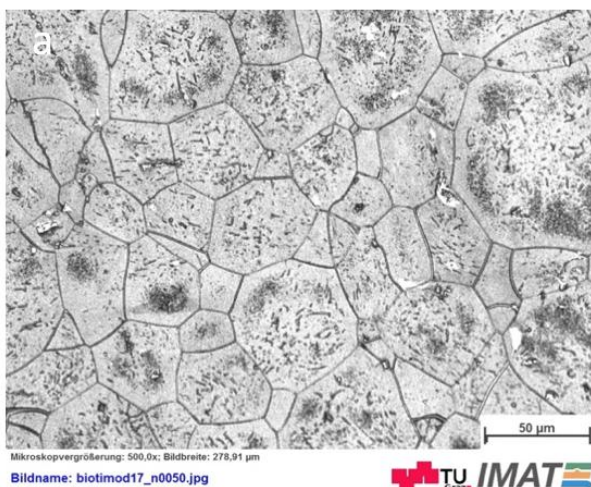


Figure 5.12: LOM images of samples heated to 500°C with 5K/min for 4 hours, 30 μm, base material (a), surface (b)

The solution of the etching for sample in figure 5.13 and 5.14 was 85 ml distilled H₂O, 10 ml hydrofluoric acid, 5 ml nitric acid for a period of 3 seconds for each sample. After the etching it is possible to observe the α phase, specially in the grain boundary. For the samples heated up to 600°C the alphas are very well observed, while in the 500°C ones are less visible.

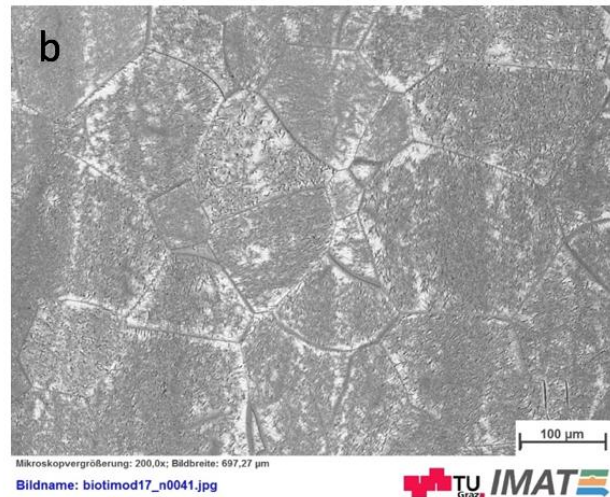
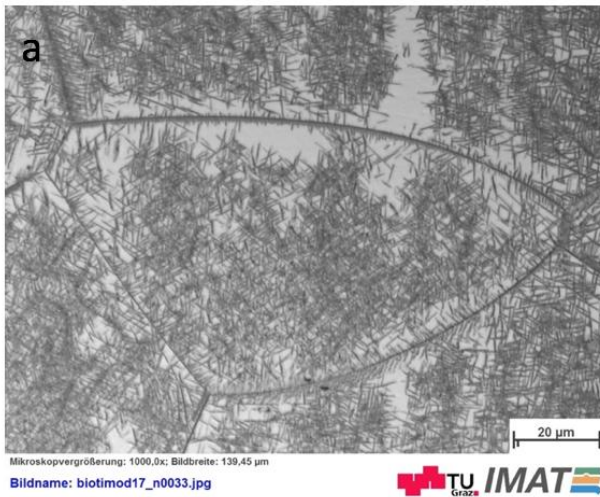


Figure 5.13: LOM images of samples heated to 600°C with 50K/min for 2 hours in base materials

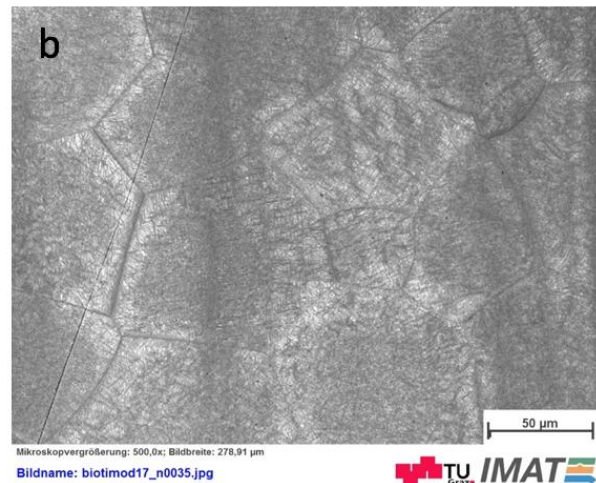


Figure 5.14: LOM images of samples heated to 550°C with 300K/min for 4 hours in base materials

5.4 Surface roughness

The following table shows the roughness, average and standard deviation measurements for each sample, moreover for structured samples the measurements were taken in 2 directions (parallel to the high short side of the sample and parallel to the long side). This double measurement was used to determine the direction of the grooves, which was found to be parallel to the short side.

Table 5.1: Roughness values (μm) obtained by profilometer

Ra (μm)	MP	EB 10		EB 30	
	0,0584	short side	long side	short side	long side
	0,0539	0,3152	0,1463	0,1887	0,2172
	0,0727	0,2511	0,1185	0,2332	0,2233
	0,0686	0,1750	0,1769	0,2292	0,2524
Mean	0,0634	0,2471	0,1472	0,2170	0,2310
SD	0,0087	0,0701	0,0292	0,0246	0,0188

Table 5.2: Roughness values (μm) obtained by profilometer, heat-treated samples

Ra (μm)	MP HT	EB 10 HT		EB 30 HT	
		short side	long side	short side	long side
	0,0469	0,3062	0,2807	0,1908	0,28
	0,0496	0,2637	0,2555	0,1790	0,1973
	0,0625	0,3262	0,3022	0,1802	0,2020
Mean	0,053	0,2987	0,2795	0,1833	0,2264
SD	0,0083	0,0319	0,0233	0,0064	0,0464

As expected, roughness increases significantly compared to smooth samples. Both EB 10 and EB 30 samples show a roughness of around $0.2 \mu\text{m}$, i. e. at the limit of the range reported in the literature as useful to avoid increasing bacterial adhesion compared to a smooth surface. In the graph below it is possible to observe roughness values for each sample type in comparison.

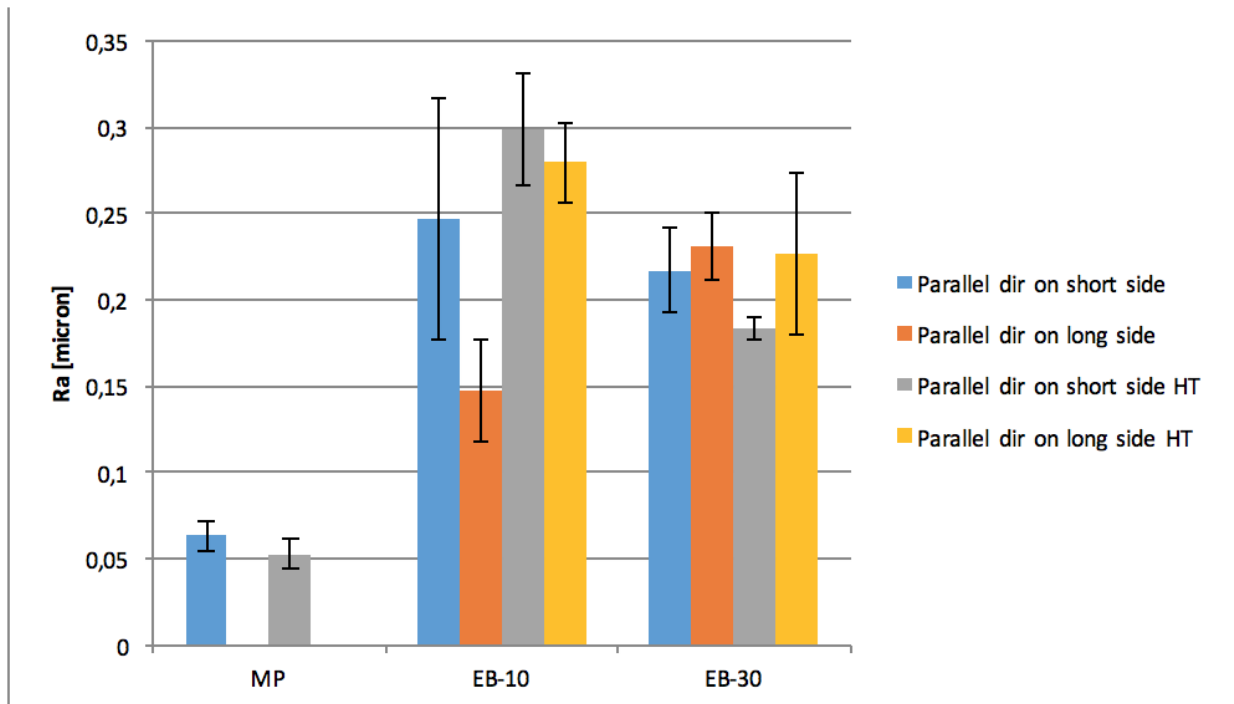


Figure 5.15: Roughness values (μm)

Three-dimensional images were obtained using an optical profilometer. From the EB 10 sample images (Fig. 5.16) it is possible to observe the grooves well on the non-heat treated sample, and also the grain boundaries are clearly visible in this case. However, areas with a higher roughness are observed at the grain boundaries. After heat treatment (Fig.5.16 b), the grains are no longer distinguishable due to a change in the microstructure of the sample: the material is full of alpha phase. Also in the EB 30 sample (Fig. 5.17) the grains are no longer visible after heat treatment, while it's still possible to identify the grooves.

In both cases, a change in roughness can therefore be observed as a result of heat treatment, the grains are clearly visible in non-heat-treated samples and the grooves are visible in both samples, but are more marked in EB 30, as shown in previous SEM analyses.

▪ **EB 10**

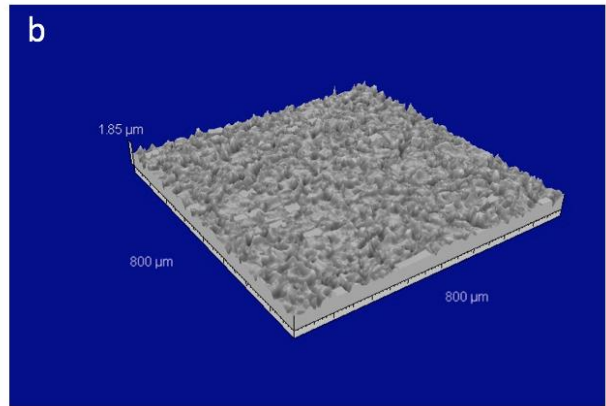
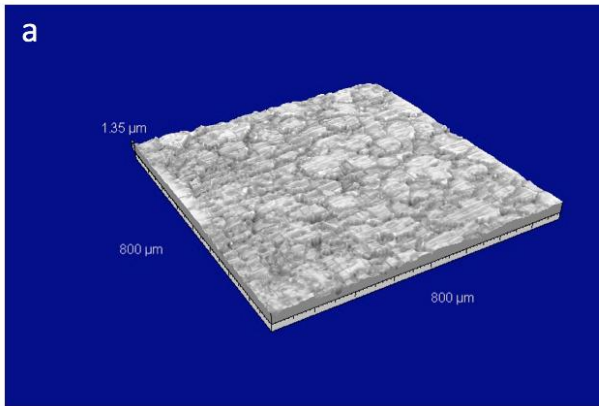


Figure 5.16: Three-dimensional view of the EB 10 (a) and EB 10 HT (b) sample surface

▪ **EB 30**

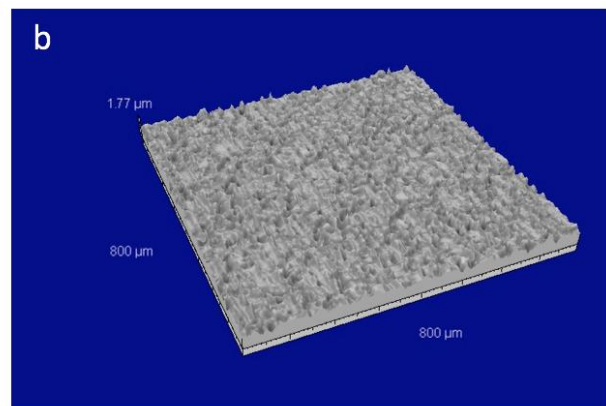
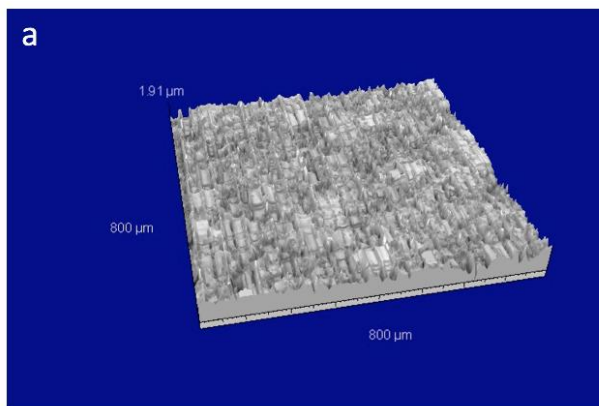


Figure 5.17: Three-dimensional view of the EB 30 (a) and EB 30 HT (b) sample surface

5.5 AFM

The results of atomic force microscope analysis analysis for samples EB 10 and EB 30 are shown below.

EB30

For the EB 30 sample, two images were obtained after scanning: 2D and 3D one. From the images it can be seen that the grooves made with electron beam have a strong preferential direction. Grooves distance is not uniform: in fact, while grooves in the centre have a distance of 30 μm , the lateral grooves seem to have a smaller distance (Fig. 5.18), probably due to defects in the grooves production phase. The grains are quite large due to the heating of the material by the laser during scanning, and it is also possible to observe a light colour impurity at the top of the image. Alongside the 2D image, from which the distance between the grooves can be easily observed, it can view the colour scale with the respective depths. From the 3D image (90 x 90 μm) it is possible to have a perfect reconstruction of the surface topography.

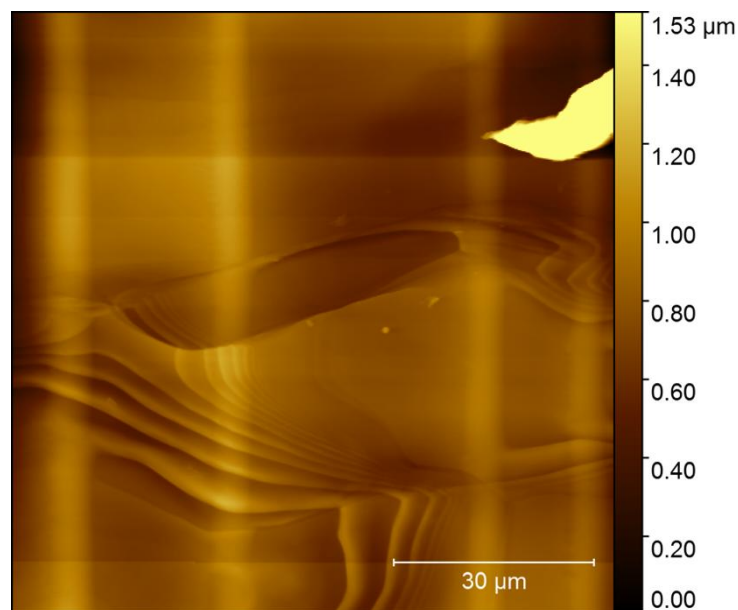
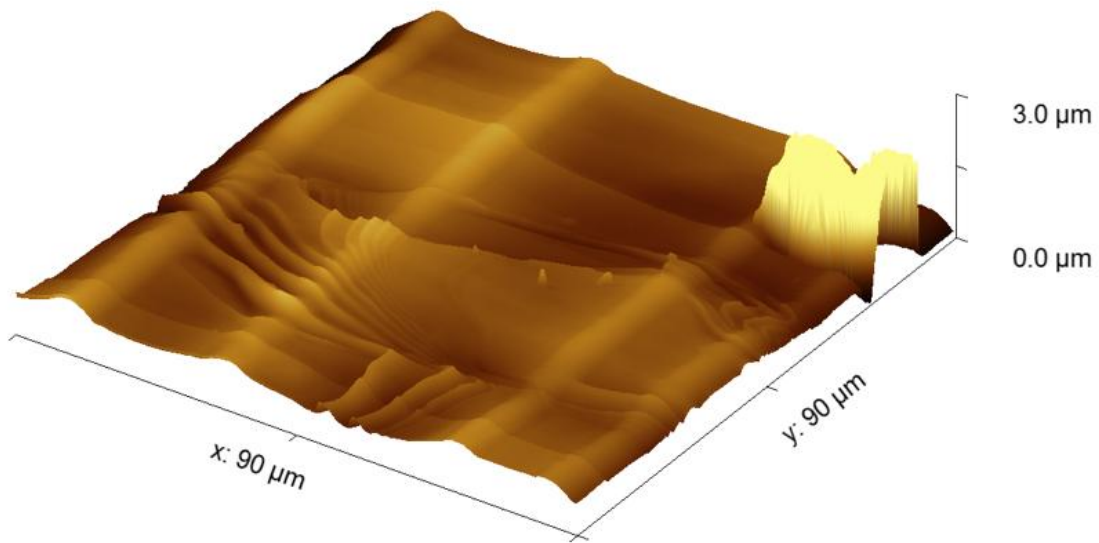


Figure 5.18: 2D image of AFM analysis, sample EB30



5.19: 3D image of AFM analysis, sample EB30

Figure

The two-dimensional profile was also determined for the EB 30 sample. From this picture it is even more evident that the distance between grooves is not homogeneous. From the image 5.20 it is also observable the depth and width of the grooves.

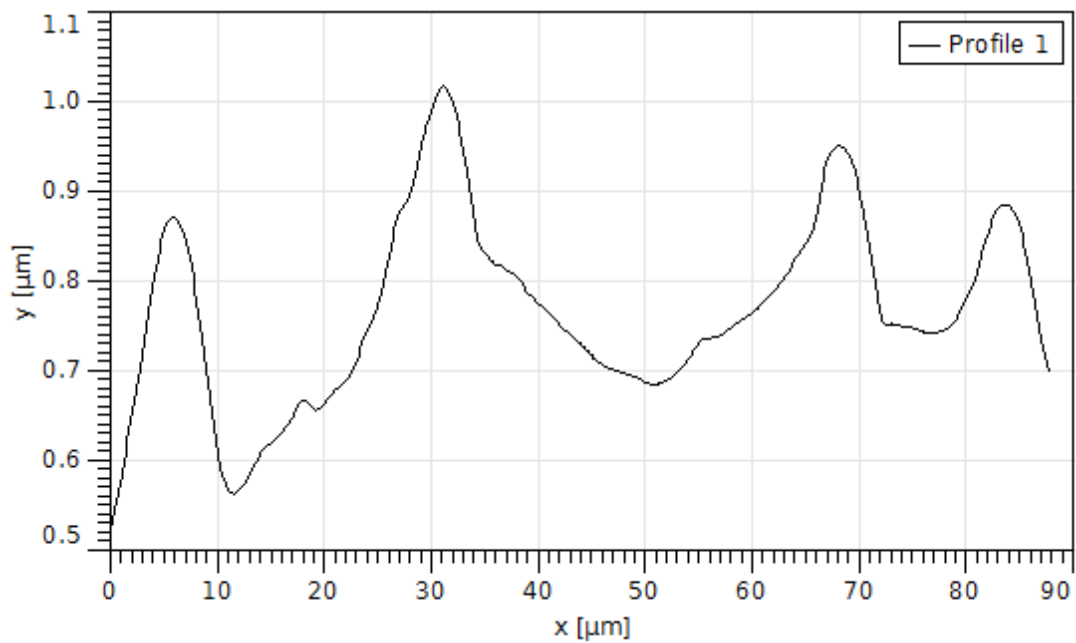


Figure 5.20: two-dimensional view of the EB 30 sample

To estimate the depth of the grooves, various measurements were made on the distance between the highest and deepest point on the surface. The results are shown in the following table.

Table 5.3: Deep values grooves

Depth (nm)	
300	
450	
330	
266	
210	
150	
Average	284,3 nm

Finally, the Ra roughness was measured both by not considering the impurity and considering it (Table 5.4). The latter values were found to be more similar to the roughness values previously estimated.

Roughness without impurity	Roughness with impurity
Ra = 123 nm	Ra = 147 nm
Rms = 156 nm	Rms = 248 nm

Table 5.4. Sample roughness without and with impurities

EB10

Much less information can be obtained from samples with grooves spaced 10 μm . In this case, in fact, the grooves are not visible after the scan. At first, 90 x 90 μm area was analysed (Fig. 5.21), but only grains are visible from the image. Then a zoom inside a grain was made trying to locate the grooves: obtaining the image 30 x 30 μm (Fig. 5.22). From the latter image we can observe two lateral depressions that recall the morphology of the grooves, but this is only a supposition and furthermore the depressions can be an effect of the laser.

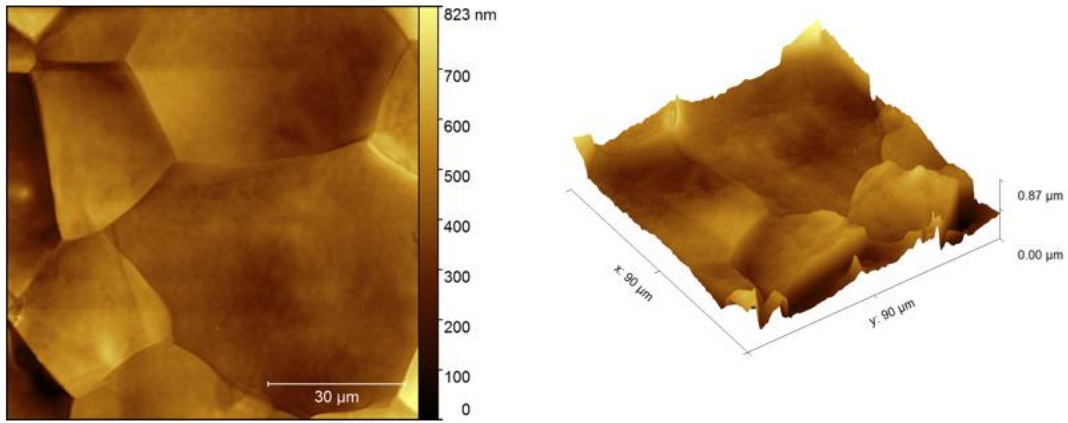


Figure 5.21: 2D and 3D image of AFM analysis, sample EB10, dimensions 90 x 90 μm

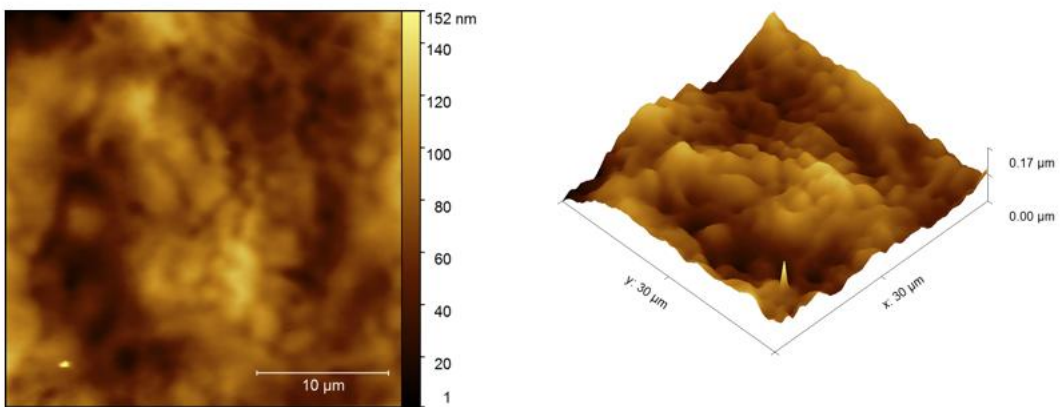


Figure 5.22: 2D and 3D image of AFM analysis, sample EB10, dimensions 30 x 30 μm

Despite the scarcity of the analysis, the roughness and depth values were also determined in this case. However, these data are not as reliable as in the previous case because the analysis did not identify the grooves.

Image 90 x 90	Image 30 x 30
Ra: 77 nm	Ra: 17 nm
Rms: 100 nm	Rms: 21 nm
	Depth: 77 nm, 82 nm

Table 5.6: depth and roughness values sample 10 μm

5.6 Contact angle

The results of contact angle measurements are shown below (table 5.7).

MP	EB 10	EB 30	MP HT	EB 10 HT	EB 30 HT
96	110,7	84,6	65	52,6	50,7
88,6	91,4	88,4	60,6	54,9	58
116,4	90	86,8			
109,1					
AVERAGE					
102,52	97,37	86,6	62,8	52,6	50,7
DEVIATION STANDARD					
12,55	11,57	1,9	3,11	1,63	5,16

Table 5.7: contact angle, mean and standard deviation measurements (degree)

For the sample non-subject to heat treatment the smooth surface, taken as a reference, results in the least wetting surface with a higher contact angle. For the EB 10 sample, the contact angle decreases but the surface is still hydrophobic, as in the previous case. As regards the EB 30 sample, this results in higher wettability and since the contact angle is less than 90 degrees the surface is hydrophilic. A clear decrease in the contact angle is observed for samples subjected to heat treatment: in this case all surfaces are hydrophilic. Therefore, an increase in wettability is observed for heat-treated specimens.

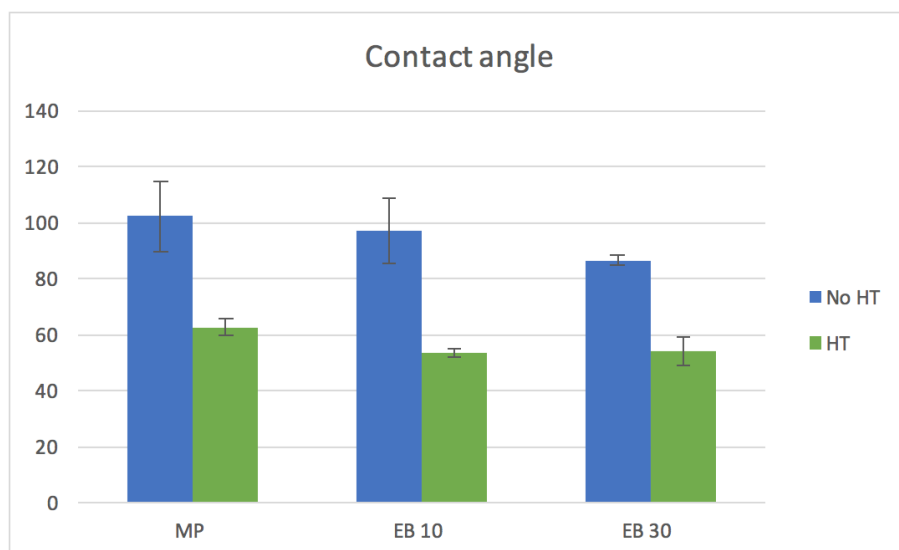


Figure 5.23: Static contact angle measured on the three sample type

5.7 XRD

XRD was used to perform an analysis to identify the crystalline phases of the Ti15Mo samples. The graph in figure 5.24 was obtained from the analysis of the diffraction spectra carried out with the *XPERT High Score* software in which the significant peaks were identified and then exported to an Excel file. Furthermore, the graph is normalized against the reference sample's main peak (MP) in order to compare the intensity of the other peaks. For all three samples the peaks obtained were typical peaks of a centred body cubic structure of titanium, confirming that samples are beta titanium alloy. The exact peak values are reported in the table 5.8 for each sample type analysed. The peaks obtained are very similar in the three cases. It is possible to observe that the main peak of the MP reference sample is slightly shifted from the other two samples: this shift may be due to the fact that the sample is not perfectly flat after polishing.

Ti15Mo MP	Ti15Mo EB10	Ti15Mo EB30
38,3657	38,8572	39,0371
55,6609	56,3483	56,3293
70,1198	70,4871	70,6981

Table 5.8: peak values for different types of samples

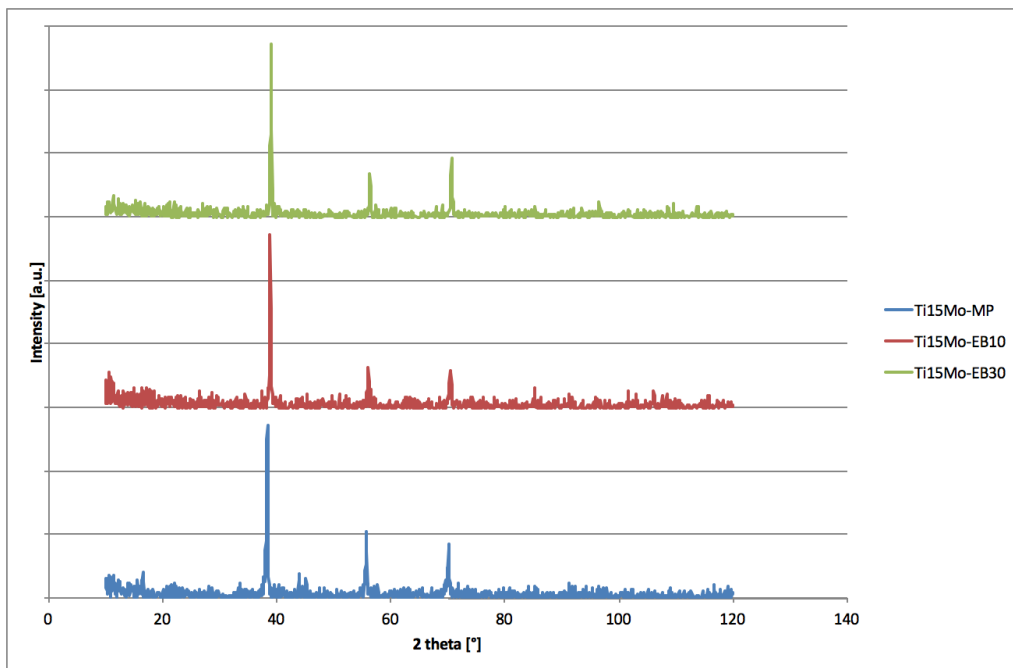


Figure 5.24: Diffraction spectrum Ti15Mo normalized to the main peak of the MP sample

From the amplitude of the main peak (Fig 5.25) it is possible to obtain information on the size of the grains. For the MP reference sample only one large peak is observed, while for the EB 10 and EB 30 the amplitude is narrowed and two peaks can be distinguished. This is due to the fact that there is not only one wavelength in the incident beam but two wavelengths. In the case of EB 10 and EB 30 the grains are larger so the spectrum shows two peaks because it highlights the presence of two λ different in the incident beam, which produce two diffraction signals and slightly different angles. When the grains are small, the peaks are wider because it is not possible to distinguish the two signals caused by the two λ . Therefore, the width of the peak depends on the size of the grains: the larger the grains, the narrower the diffractometric peaks. It is possible to observe a growth of the grains in samples subjected to electron beam: in fact, the laser causes a strong heating of grains and this process tends to make them grow. This effect can only be seen on the main peak because the others are too small.

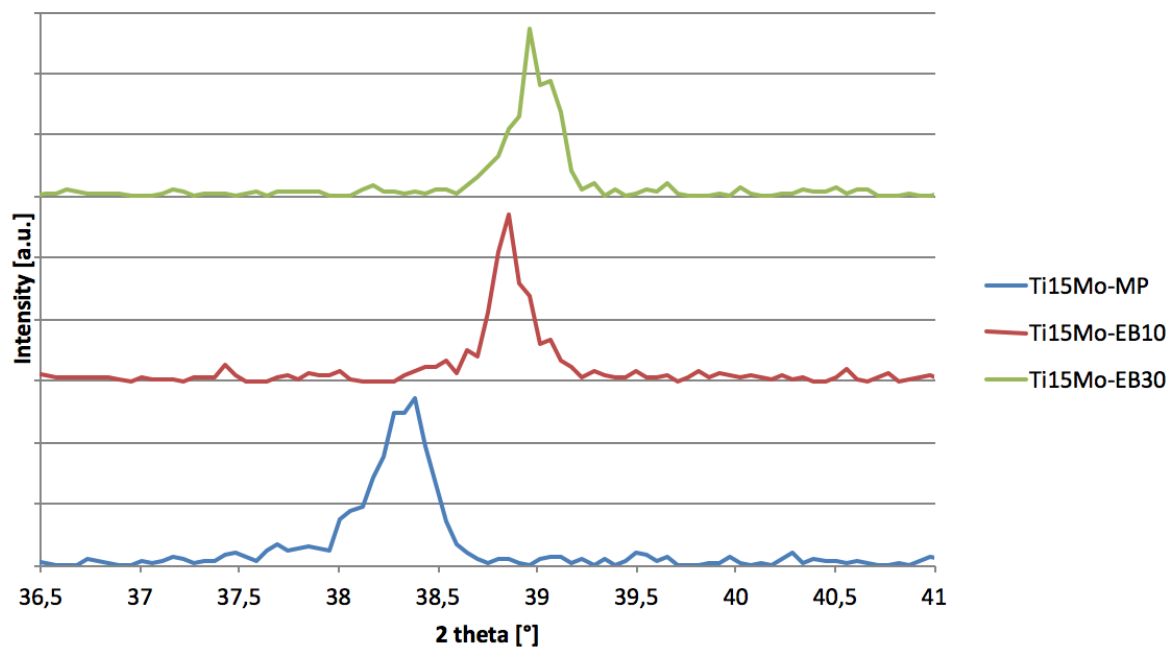


Figure 5.25: Amplitude of the main peak in the three samples

5.8 Cell and bacteria test

Cell viability tests show that grooves do not induce cytotoxicity (Fig. 5.26). To verify the alignment (Fig. 5.27), the cells have been marked with fluorescent markers that bind to the nucleus and cytoskeleton; in this way it is possible to see how the cell body is oriented. The best orientation is for the sample EB 10 in fact the cells are oriented to the grooves. In the EB 30 sample, orientation is partial: zones with cells oriented and zones where orientation is absent are alternated. For the smooth sample, however, the orientation is random. It seems therefore that even if the 10 μm grooves are not so visible and uniform in the analyses previously carried out, the cells feel them uniformly on the whole sample and tend to align the cytoskeleton to the grooves.

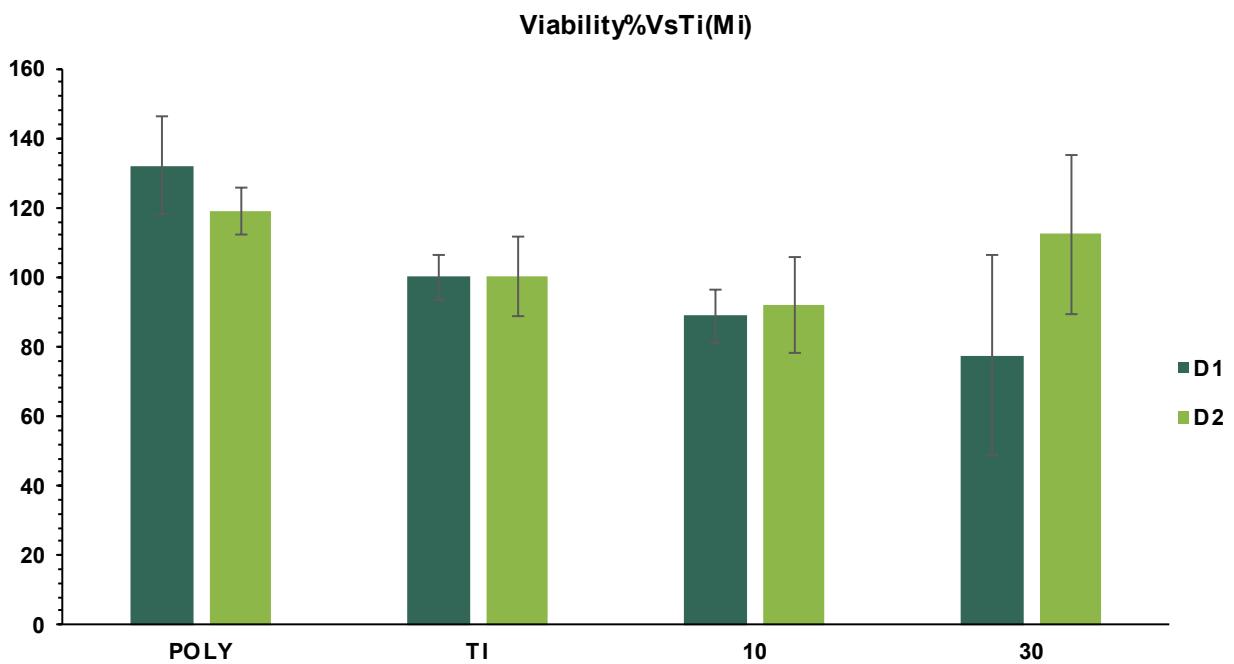


Figure 5.26: HGF viability analysis

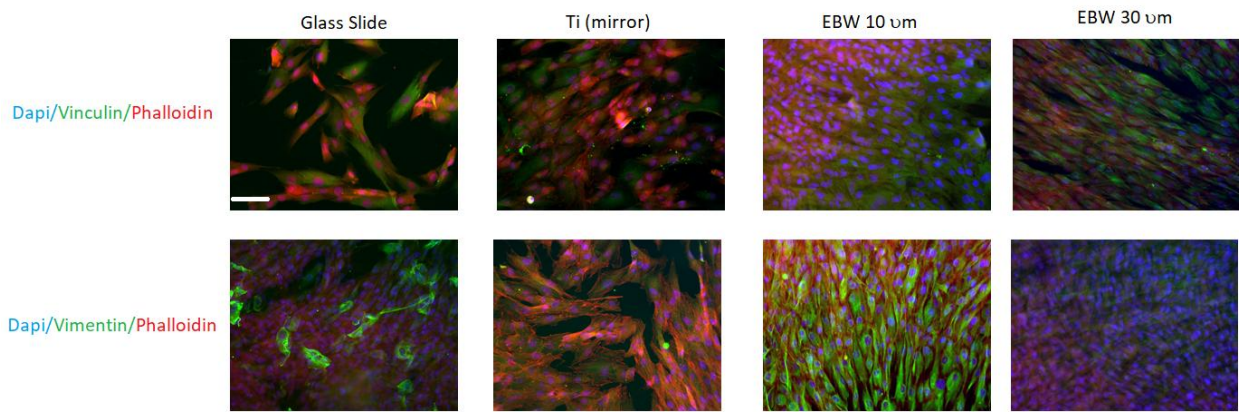


Figure 5.27 Cell alignment for different sample types: Cytoskeleton appears aligned to nanogroves when HGF are growth on Ti treated with EBW. However, the effect is highlighter with EBW10

Finally, grooves do not increase bacterial adhesion compared to the smooth surface (they are therefore suitable for the purpose), but there is no decrease in bacterial adhesion on structured samples: EBW technique have no antibacterial or bacteriostatic effect. The number of bacteria present on the sample surface was evaluated by counting the colonies forming units (CFU).

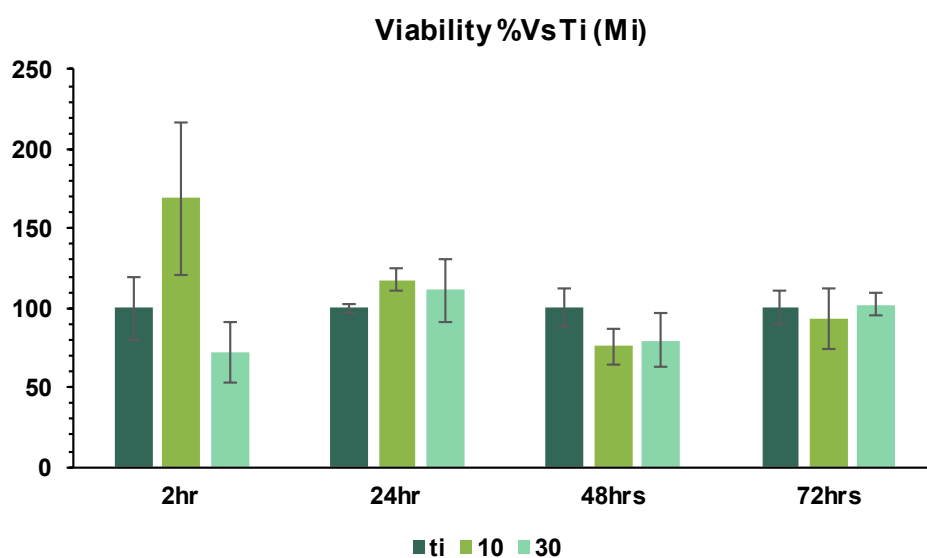


Figure 5.28: bacterial viability analysis

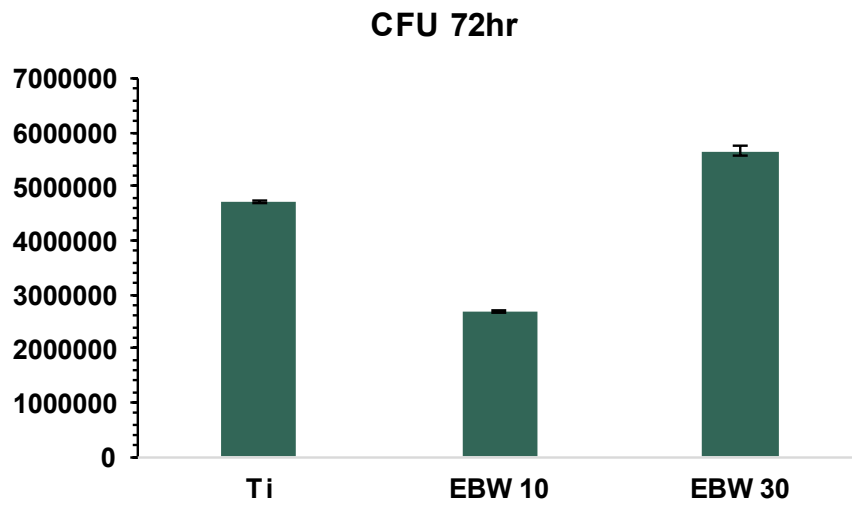


Figure 27.29: counting bacteria on samples after 72 hours

Conclusion and future works

The objective of this thesis work was to perform surface modifications on dental implant neck made of titanium to promote cellular adhesion and prevent bacterial adhesion. In this regard a beta titanium alloy was used to obtain finer grains than pure titanium. The Ti15Mo alloy samples were grinding and polished at the Technical University of Graz. The samples were then surface modified using electron beam, in order to create parallel grooves spaced 10 μm and 30 μm from each other. Subsequently, part of the microstructured samples were heat treated to obtain alpha phase precipitation and consequently a biphasic alloy. The samples were then subjected to surface characterization at the Technical University of Graz (SEM) and at the Politecnico di Torino (Surface roughness, AFM, wettability, XRD) and to cellular and finally cell and bacterial tests were carried out at the Univesità del Piemonte Orientale Amedeo Avogadro.

SEM analyses of the samples subjected to electron beam showed the effective presence of grooves: these were more visible for samples with grooves 30 μm apart than for those with 10 μm spacing. Moreover, thanks to the SEM analysis it was possible to verify the presence of the alpha phase following the heat treatments: this phase was uniformly distributed over the whole sample but with a denser distribution on beta grain boundary.

The average roughness of the samples was around 0.2 μm and therefore is within the limit reported in the literature as useful for not increasing bacterial adhesion compared to a smooth surface. In addition, the heat-treated samples have a higher roughness due to changes in the material microstructure (alpha phase precipitation). This change in roughness was observed thanks to the profilometer images, which also showed that the 10 μm microstructure was more evident compared to SEM images.

The profile of the grooves was reconstructed by AFM, in this case the measurements were reliable only for the sample with 30 μm grooves because for the sample with a microstructure of 10 μm it was not possible to observe the grooves. The average depth of the grooves spaced 30 μm was then measured and was 284.3 nm, in line with the values found in the literature. These analyses were only performed on samples that were not heat treated.

Contact angle measurements showed an increase in wettability for heat treated samples compared to non-heat treated samples. In both cases, a decrease in the contact angle is observed for the structured samples compared to the mirror polished reference.

From the X-ray analyses it was possible to highlight the crystalline phases of the samples. For non-heat-treated samples, only the beta phase was present, confirming that the samples are a titanium beta alloy. Furthermore, by analyzing the amplitude of the peaks found, it was possible to verify an increase in the size of the grains in the structured samples compared to the smooth samples due to the heating to which the material was subjected during surface modification using electron beam.

Finally, thanks to cellular and bacterial testing, the material and grooves were found to be non-toxic, as expected. Grooves do not increase bacterial adhesion compared to the smooth surface, but there is no decrease in bacterial adhesion on structured samples. Regarding the effect of bacterial adhesion, the best alignment was found to be on the 10 μm grooves.

In conclusion, it can be said that grooves made with 10 μm EB are the best to obtain adhesion and cell alignment, although the surface characterization analysis showed that the 30 μm grooves were the most visible. In addition, the samples do not exhibit an antibacterial or bacteriostatic effect, but they do not show an increase in bacterial adhesion compared to the smooth surface. They are therefore suitable for the purpose.

An interesting future work would be to evaluate how heat treated samples affect the adhesion of cells and bacteria. Following the heat treatment, in fact, a variation of the microstructure of the samples and an increase in roughness are observed, which would certainly affect the cellular and bacterial behaviour.

Bibliography

- [1] G. Anastasi, *Trattato di anatomia umana*. Edi. Ermes, 2006.
- [2] R. Kalluri and M. Zeisberg, "Fibroblasts in cancer," *Nature Reviews Cancer*, vol. 6, no. 5. pp. 392–401, 2006.
- [3] J. J. Tomasek, G. Gabbiani, B. Hinz, C. Chaponnier, and R. A. Brown, "Myofibroblasts and mechano-regulation of connective tissue remodelling," *Nat. Rev. Mol. Cell Biol.*, vol. 3, no. 5, pp. 349–363, 2002.
- [4] R. Bedini *et al.*, "Protocollo preliminare di analisi microtomografica in vitro dell'interfaccia osso-impianto dentale," *Ippolo*, vol. 8539, 2009.
- [5] Fallschussel G.K.H, *Implantologia odontoiatrica: teoria e pratica*, Edinava. 1989.
- [6] Annarita Signoriello, "OSTEOINDUCTIVE TITANIUM SURFACES IN ORAL IMPLANTOLOGY," UNIVERSITA' DEGLI STUDI DI PADOVA – FACOLTA' DI INGEGNERIA, 2010.
- [7] T. Berglundh and S. Göteborg, "TESSUTI MOLLI PERI-IMPLANTARI E PARODONTALI."
- [8] K. Arvidson, H. Bystedt, A. Frykholm, L. von Konow, and E. Lothigius, "Five-year prospective follow-up report of the Astra Tech Dental Implant System in the treatment of edentulous mandibles," *Clin. Oral Implants Res.*, vol. 9, no. 4, pp. 225–234, 1998.
- [9] a Quaranta, C. Maida, A. Scrascia, G. Campus, and M. Quaranta, "Er:Yag Laser application on titanium implant surfaces contaminated by *Porphyromonas gingivalis*: an histomorphometric evaluation.," *Minerva stomatologica*, vol. 58, no. 7–8. pp. 317–30, 2009.
- [10] "La mucosità perimplantare e la perimplantite: il loro ruolo nella patologia implantare :Dental Tribune Italy." [Online]. Available: <https://it.dental-tribune.com/clinical/la-mucosita-perimplantare-e-la-perimplantite-il-loro-ruolo-nella-patologia-implantare/>. [Accessed: 12-Mar-2018].
- [11] "https://en.wikipedia.org/wiki/Gram-negative_bacteria." .
- [12] "MEDICINA ONLINE | Salute del fisico, benessere della mente, bellezza del corpo. Articoli monotematici di medicina, scienza, cultura e curiosità." [Online]. Available: <https://medicinaonline.co/>. [Accessed: 12-Mar-2018].
- [13] J. Ata-Ali, M. E. Candel-Marti, A. J. Flichy-Fernández, D. Peñarrocha-Oltra, J. F. Balaguer-Martinez, and M. P. Diago, "Peri-implantitis: Associated microbiota and treatment," *Medicina Oral, Patologia Oral y Cirugia Bucal*, vol. 16, no. 7. 2011.
- [14] D. DI Biologia Corso Di Laurea Magistrale In Biologia Applicata Alla Biomedicina, P. Sonia

Senesi Profssa Arianna Tavanti Candidata, M. Vicari, and D. Santo Caracappa, "UNIVERSITA' DI PISA," 2013.

- [15] "Homepage - DentalAcademy." [Online]. Available: <http://www.dentaljournal.it/>. [Accessed: 12-Mar-2018].
- [16] T. F. Deuel, R. M. Senior, J. S. Huang, and G. L. Griffin, "Chemotaxis of monocytes and neutrophils to platelet-derived growth factor," *J. Clin. Invest.*, vol. 69, no. 4, pp. 1046–1049, 1982.
- [17] H. Seppa, G. Grotendorst, S. Seppa, E. Schiffmann, and G. R. Martin, "Platelet-derived growth factor is chemotactic for fibroblasts," *J. Cell Biol.*, vol. 92, no. 2, pp. 584–588, 1982.
- [18] "Osteointegrazione - Wikipedia." [Online]. Available: <https://it.wikipedia.org/wiki/Osteointegrazione>. [Accessed: 13-Mar-2018].
- [19] "Biomateriali in "Enciclopedia della Scienza e della Tecnica"," [Online]. Available: http://www.treccani.it/enciclopedia/biomateriali_%28Enciclopedia-della-Scienza-e-della-Tecnica%29/. [Accessed: 12-Mar-2018].
- [20] Q. Chen and G. A. Thouas, "Metallic implant biomaterials," *Materials Science and Engineering R: Reports*, vol. 87. pp. 1–57, 2015.
- [21] D. F. Williams, "Definitions in biomaterials: proceedings of a consensus conference of the European Society for Biomaterials," 1987.
- [22] S. Bauer, P. Schmuki, K. von der Mark, and J. Park, "Engineering biocompatible implant surfaces: Part I: Materials and surfaces," *Progress in Materials Science*, vol. 58, no. 3. pp. 261–326, 2013.
- [23] "Materiali e Biomateriali." [Online]. Available: http://people.unica.it/pau/files/2015/10/3mod-materiali_biocomp.pdf. [Accessed: 12-Mar-2018].
- [24] "Proprietà fisiche del titanio." [Online]. Available: [http://www.ing.unitn.it/~colombo/Ti in auto/Relazione per web_versione_02-07_file/Page444.htm](http://www.ing.unitn.it/~colombo/Ti%20in%20auto/Relazione%20per%20web_versione_02-07_file/Page444.htm). [Accessed: 12-Mar-2018].
- [25] C. Leyens and M. Peters, *Titanium and Titanium Alloys*. 2003.
- [26] M. Cariola, M. Gerbi Sethi, A. Nicolin, Ceris., and Istituto per la corrosione marina dei metalli., *Il titanio : un metallo per molteplici applicazioni : analisi tecnologica e valutazioni economiche*. F. Angeli, 1996.
- [27] J. Donachie and J. M., "Titanium – A Technical Guide," *ASM Int. 2nd Ed.*, vol. 55, no. 11, pp. 1023–1026, 2000.

- [28] K. Firm, R. Boyer, and G. Welsch, *Materials Properties Handbook: Titanium Alloys*. 1994.
- [29] "Titanium Alloy Guide | Titanium | Alloy."
<https://www.scribd.com/document/163670620/Titanium-Alloy-Guide>.
- [30] M. Abdel-Hady Gepreel and M. Niinomi, "Biocompatibility of Ti-alloys for long-term implantation," *Journal of the Mechanical Behavior of Biomedical Materials*, vol. 20. pp. 407–415, 2013.
- [31] J. W. Lu, Y. Q. Zhao, P. Ge, and H. Z. Niu, "Microstructure and beta grain growth behavior of Ti-Mo alloys solution treated," *Mater. Charact.*, vol. 84, pp. 105–111, 2013.
- [32] Monika Gabernig, "Surface structuring and microstructure development of a metastable beta-titanium alloy for biomedical application prepared by an electron beam technique," Graz University of Technology, 2016.
- [33] F. F. Cardoso, P. L. Ferrandini, E. S. N. Lopes, A. Cremasco, and R. Caram, "Ti-Mo alloys employed as biomaterials: Effects of composition and aging heat treatment on microstructure and mechanical behavior," *J. Mech. Behav. Biomed. Mater.*, vol. 32, pp. 31–38, 2014.
- [34] S. Kalpakjian and S. R. Schmid, *Manufacturing Engineering and Technology*. 2010.
- [35] N. Saresh, M. G. Pillai, and J. Mathew, "Investigations into the effects of electron beam welding on thick Ti-6Al-4V titanium alloy," *J. Mater. Process. Technol.*, vol. 192–193, pp. 83–88, 2007.
- [36] K. von der Mark and J. Park, "Engineering biocompatible implant surfaces: Part II: Cellular recognition of biomaterial surfaces: Lessons from cell–matrix interactions," *Progress in Materials Science*, vol. 58, no. 3. pp. 327–381, 2013.
- [37] H. F. Lodish, "Molecular cell biology," 2008. .
- [38] S. Spriano and S. Ferraris, "How topographical surface features can affect the interaction of implants with soft tissues?"
- [39] K. Anselme, P. Davidson, A. M. Popa, M. Giazon, M. Liley, and L. Ploux, "The interaction of cells and bacteria with surfaces structured at the nanometre scale," *Acta Biomaterialia*, vol. 6, no. 10. pp. 3824–3846, 2010.
- [40] S. Y. Kim, N. Oh, M. H. Lee, S. E. Kim, R. Leesungbok, and S. W. Lee, "Surface microgrooves and acid etching on titanium substrata alter various cell behaviors of cultured human gingival fibroblasts," *Clin. Oral Implants Res.*, vol. 20, no. 3, pp. 262–272, 2009.
- [41] Y. Lai *et al.*, "Effect of 3D microgroove surface topography on plasma and cellular

- fibronectin of human gingival fibroblasts," *J. Dent.*, vol. 41, no. 11, pp. 1109–1121, 2013.
- [42] G. a Dunn and a F. Brown, "Alignment of fibroblasts on grooved surfaces described by a simple geometric transformation.," *J. Cell Sci.*, vol. 83, pp. 313–40, 1986.
- [43] S. W. Lee, S. Y. Kim, I. C. Rhyu, W. Y. Chung, R. Leesungbok, and K. W. Lee, "Influence of microgroove dimension on cell behavior of human gingival fibroblasts cultured on titanium substrata," *Clin. Oral Implants Res.*, vol. 20, no. 1, pp. 56–66, 2009.
- [44] S. Fujita, M. Ohshima, and H. Iwata, "Time-lapse observation of cell alignment on nanogrooved patterns," *J. R. Soc. Interface*, vol. 6, no. Suppl_3, pp. S269–S277, 2009.
- [45] W. A. Loesberg *et al.*, "The threshold at which substrate nanogroove dimensions may influence fibroblast alignment and adhesion," *Biomaterials*, vol. 28, no. 27, pp. 3944–3951, 2007.
- [46] E. Eisenbarth, J. Meyle, W. Nachtigall, and J. Breme, "Influence of the surface structure of titanium materials on the adhesion of fibroblasts," *Biomaterials*, vol. 17, no. 14, pp. 1399–1403, 1996.
- [47] K. Bohinc *et al.*, "Metal surface characteristics dictate bacterial adhesion capacity," *Int. J. Adhes. Adhes.*, vol. 68, pp. 39–46, 2016.
- [48] A. Al-Ahmad *et al.*, "In vivo study of the initial bacterial adhesion on different implant materials," *Arch. Oral Biol.*, vol. 58, no. 9, pp. 1139–1147, 2013.
- [49] K. J. Edwards and A. D. Rutenberg, "Microbial response to surface microtopography: The role of metabolism in localized mineral dissolution," *Chem. Geol.*, vol. 180, no. 1–4, pp. 19–32, 2001.
- [50] L. C. Xu and C. A. Siedlecki, "Submicron-textured biomaterial surface reduces staphylococcal bacterial adhesion and biofilm formation," *Acta Biomater.*, vol. 8, no. 1, pp. 72–81, 2012.
- [51] https://it.wikipedia.org/wiki/Microscopio_elettronico_a_scansione.
- [52] "https://en.wikipedia.org/wiki/Surface_roughness." .
- [53] G. Binnig, C. F. Quate, and C. Gerber, "Atomic Force Microscope," *Phys. Rev. Lett.*, vol. 56, no. 9, pp. 930–933, Mar. 1986.
- [54] D. Ssa and L. Basiricò, "Forze di interazione tra particelle e superfici," 2010. .
- [55] http://www.enea.it/it/Ricerca_sviluppo/documenti/ricerca-di-sistemelettrico/combustibili-fossili-ccs/2012/rds-2013-210.pdf.